

Experiments on Hydrogen Engine Exhaust After-Treatment Systems

VICTOR BERG

Department of Mechanics and Maritime Sciences

CHALMERS UNIVERSITY OF TECHNOLOGY

Gothenburg, Sweden 2025

Contents

1	Introduction	2
2	Experimental Setup	4
2.1	Engine	4
2.2	Exhaust Aftertreatment System.....	5
2.3	Measurement Equipment.....	9
2.4	Design of Experiments.....	12
2.5	SCR Evaluation	13
3	Results	15
3.1	Engine-Out Emissions & Oxidising Catalyst Performance	15
3.2	SCR Catalyst Performance	18
4	Discussion.....	27
4.1	Limitations.....	27
5	Conclusions	28
	References	29
	Abbreviations.....	30
	Appendix 1: Urea Calibration Data	31
	Appendix 2: SCR Measured Data.....	33
	Appendix 3: Additional SCR plots.....	34
	Appendix 4: Model Data for Catalyst.....	39

1 Introduction

Hydrogen is a potential future fuel due to its carbon free nature. Provided that the hydrogen is produced from carbon free electricity it can play an important role in a future transport solution.

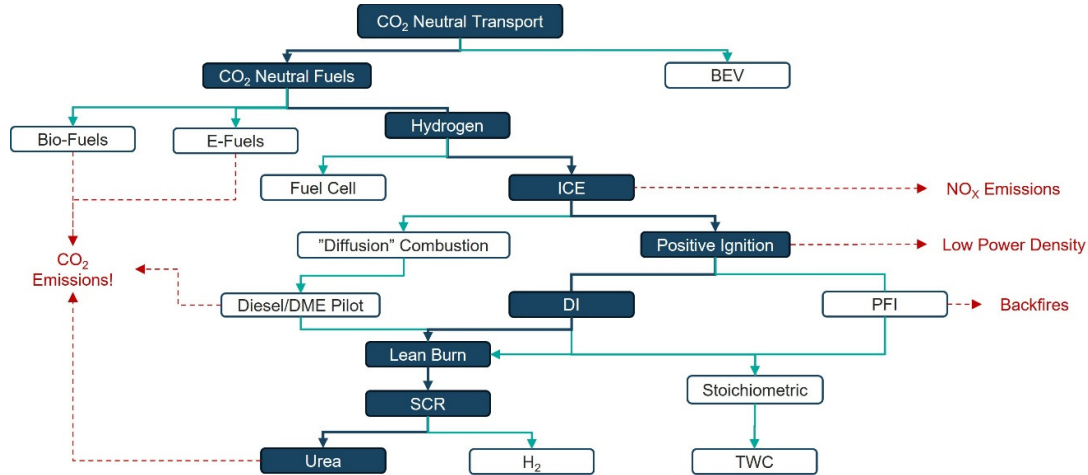


Figure 1: Overview of low CO₂ transport technologies

An overview of different technological solutions for potentially CO₂ neutral transport is shown in Figure 1, where the red lines and labels indicate some of the major downsides of the concepts. Hydrogen stands out as one of the few fuels that can achieve close to zero tailpipe CO₂ emissions.

There are several technological solutions for a hydrogen internal combustion engine. One that has seen relatively large interest lately is different forms of compression ignition or compression ignition-like combustion systems, with potentially very high efficiency [1-5].

Dual-fuel systems typically combine hydrogen with a carbon-containing fuel that is used as an ignition improver or a pilot fuel to ensure combustion if the hydrogen that is often injected close to top dead centre (TDC) [1, 6].

One hurdle with these approaches is the feasibility of high-pressure direct injection of hydrogen, something that puts high demands on the injectors and may require a booster pump onboard the vehicles to maintain operation when the tank pressure is reduced.

An alternative approach, that was commonly used in early research on hydrogen engines, is the use of port fuel injection in a spark ignition engine. This however has potential drawbacks in the form of low specific power [6], as well as some risks involved when it comes to backfires etc. The benefits are low emission and the ability to run on pure hydrogen.

The third approach could be considered a middle of the road approach. By using direct injection at lower injection pressures, the need for a booster pump in the fuel system can be reduced. Injection can also take place after intake valve closing (IVC), which

avoids the loss of power due to hydrogen displacing the intake air. Injecting fuel after IVC would also remove the risk of backfires.

The reduced technical demands on the intake system could enable a quicker adoption of this approach, however, it is not without its challenges. The late injection leads to less time for hydrogen and air mixing, which poses issues for the combustion stability and knock mitigation.

Another issue that is the focus of this paper is the engine out emissions, which can be high in nitrogen oxides (NO_x). An approach that is attractive is to lean out the hydrogen mixture enough to reduce engine out emissions to acceptable levels [6, 7]. This typically reduces power density of the engine, which is already a challenge for most spark ignition concepts. Lean combustion also poses challenges for a potential turbo [8-10], as the lean mixtures will produce exhaust of low specific enthalpy while high intake air flows at high pressures will be required.

Apart from strategies to lower engine out emissions, an exhaust aftertreatment system (EATS) may be needed. A selective catalytic reaction (SCR) catalyst can be used to reduce the NO_x emissions of a hydrogen engine, and has been proven to be able to reduce the emissions to the legal limit, both in stationary tests [8] and in the WLTC drive cycle [11].

An SCR system may also include an upstream oxidising catalyst. Traditionally, this has been used to oxidise the hydrocarbon and carbon monoxide emissions, of which a hydrogen engine produces very little, but an important function is to oxidize NO into NO_2 , which in turn benefits the SCR catalyst as it enables the fast reduction pathway of nitrogen oxides.

The exhaust gases from a hydrogen engine operated at lean conditions will generally be cold, which could prevent the heat up of the catalyst.

The paper aims to answer the following questions:

What impact does operating parameters have on the following

- Engine out emissions
- Oxidising catalyst functionality
- SCR efficiency

2 Experimental Setup

2.1 Engine

The engine used in this study is a heavy-duty hydrogen engine, based on an AVL research engine. The single cylinder engine is typical of those found in commercial diesel trucks, apart from modifications made to operate the engine in hydrogen. A summary of some of the engine properties is shown in Table 1.

Table 1: Engine data

Engine Specifications		
Displacement	2.13	dm ³
Bore	131	mm
Stroke	158	mm
Conrod length	259	mm
Compression ratio	10.5:1	-

The most important changes made to the engine is a prototype piston the lowers the compression ratio from the 17:1 ratio typically used in this type of engines to 10.5:1, similar to a typical SI engine. The new piston also lacks the typical diesel bowl. The head has also been modified to allow the fitting of a spark plug and a prototype, single hole hydrogen injector.

The fuel supply consists of tanks of compressed hydrogen, a pressure regulator controlled by a programmable logic controller, stainless steel lines and a small buffer tank just upstream of the injector. The function of the buffer tank is to avoid sharp pressure drops during injections, by allowing a larger volume of hydrogen close to the injector. This also simplifies the operation of the pressure regulator, as the pressure at the hydrogen bottles fluctuates less. The engine is shown in Figure 2. The hood over the engine is used to capture any escaped hydrogen and connected to a fan. To the right is the large plenum used diminish the effects of the pressure pulses in the intake. Hidden behind the engine in the picture, is a similar, but larger volume that is used to reduce the effects of the pressure pulses in the exhaust. The hydrogen line enters the picture from the left, and is connected to the hydrogen buffer tank mounted above where the air intake connects to the cylinder head.



Figure 2: Heavy duty research engine.

Test bed operation is controlled by an AVL PUMA system, and all engine operating parameters, such as speed, timings of injection and spark as well as intake and exhaust pressure are set manually. The parameters that were changed in this study included spark timing, intake and exhaust pressures and dyno speed. Other settings, such as intake temperature, spark currents and fuel pressures were set as constants. Unsteady injection rates also meant that the injection duration needed to be adjusted from time to time during operation, even though the goal was to maintain a constant amount of fuel injected per cycle.

The intake temperature, intake pressure, exhaust backpressure and fuel pressure were controlled to their respective setpoints using PID controllers.

2.2 Exhaust Aftertreatment System

The engine was fitted with an exhaust aftertreatment system consisting of an oxidising catalyst and a selective catalytic reduction system.

The exhaust aftertreatment system (EATS) is simplified compared to those found on commercial vehicles and the commonly used particle filter and ammonia slip catalyst are missing. As schematic layout of the system is shown in Figure 3:

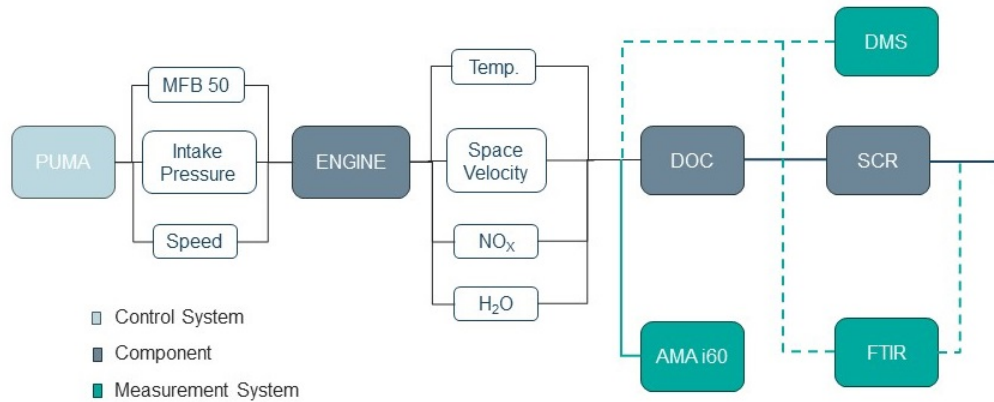


Figure 3: Schematic layout of the engine, exhaust, and key measurement equipment. Dashed lines mean movable connection, while solid lines indicate a fixed mounting.

The main properties of the gas stream that are of interest are shown in the branched boxes in the figure above. The hardware components and their relative position are shown through the dark grey boxes, while the measurement systems and their probe locations are shown in green. For clarity, the thermocouples have been omitted from the figure. The exhaust gases flow from left to right. A picture of the physical system is shown in Figure 4.

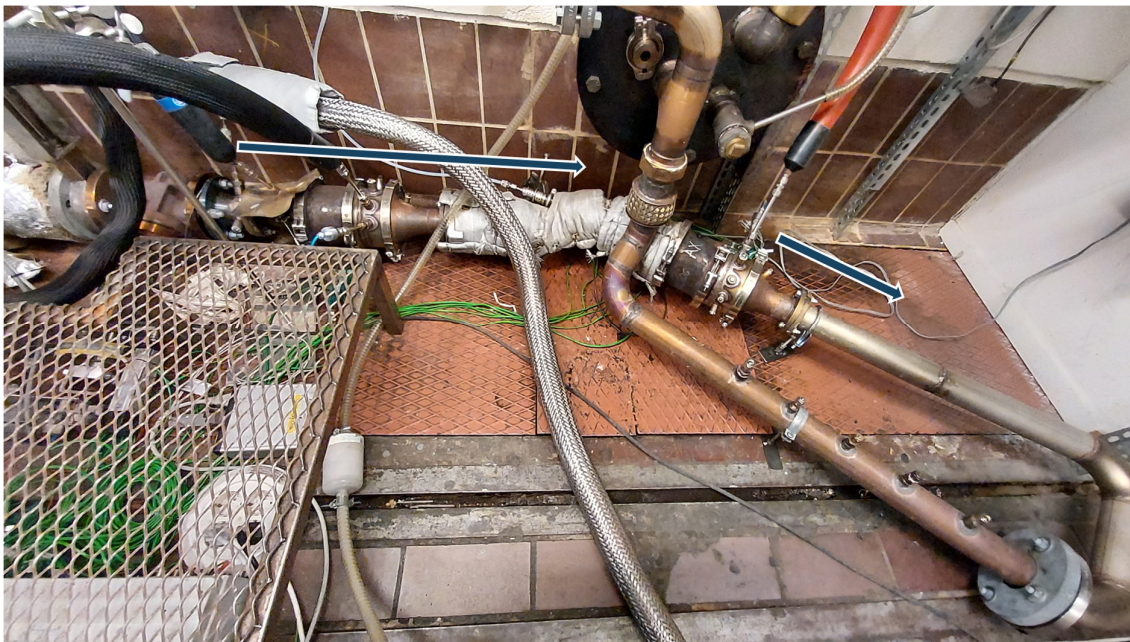


Figure 4: Exhaust aftertreatment system. The arrows indicate the flow direction.

The exhaust gases enter from the top left and flows to the right, before looping back into the central exhaust from the test cell, shown in the centre. The catalysts are the clamped sections, comprised of a conical section to increase the diameter, a cylindrical catalyst section. Clamped to the back side is a similar, but empty section that is used to hold the measuring probes for the different instruments, followed by a final cone that tapers

down to the exhaust diameter. The system is built so that the catalysts can easily be changed if needed.

2.2.1 Catalysts

The (diesel) oxidising catalyst is a titanium supported platinum catalyst, with a loading of $40\text{g}/\text{ft}^3$. The catalyst is mounted upstream of the selective catalytic reaction (SCR) catalyst. It is a cylindrical brick mounted in a pipe with a circular cross section. The catalyst is 4.66 inches in diameter and 3 inches long, giving it a volume of approximately 850 cm^3 . To accommodate the difference in diameter between the catalyst and the exhaust pipe, conical sections are used. Just downstream of the catalyst, a measuring section with probes for a Fourier Transform Infra-Red (FTIR) analyser from IAG and DMS 500 fast particle analyser from Cambustion is mounted. The catalyst has also been prepared with temperature probes in the inlet, outlet and in three positions around the circumference.

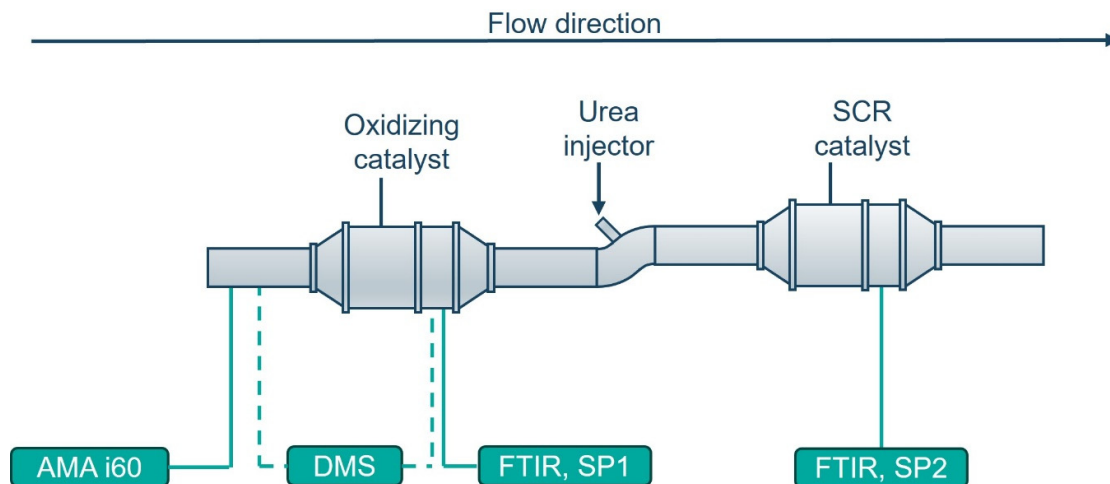


Figure 5: EATS and measurement probe positions. Dashed lines in the figure indicate temporary connections.

The SCR system consists of a copper-zeolite substrate. The formulation of the catalyst is typical of those found in commercially available catalysts. The catalyst has the same dimensions as the oxidising catalyst and is mounted in a similar sampling section. The pipe layout including measurement sections and cones is the same both catalysts, as shown in Figure 5, with the exception that neither the DMS nor the AMA i60 was mounted downstream of the SCR system for any measurements.

Both catalysts were fitted with five temperature probes each, to allow monitoring of temperature uniformity and exothermic reactions. One thermocouple was fitted to the front centre of each catalyst brick. Three additional thermocouples were fixed at equal spacing around the circumference, at the midpoint in the axial direction, while a final thermocouple was inserted in the centre at the rear edge of the brick. An illustration of the placement of the probes is shown in Figure 6.

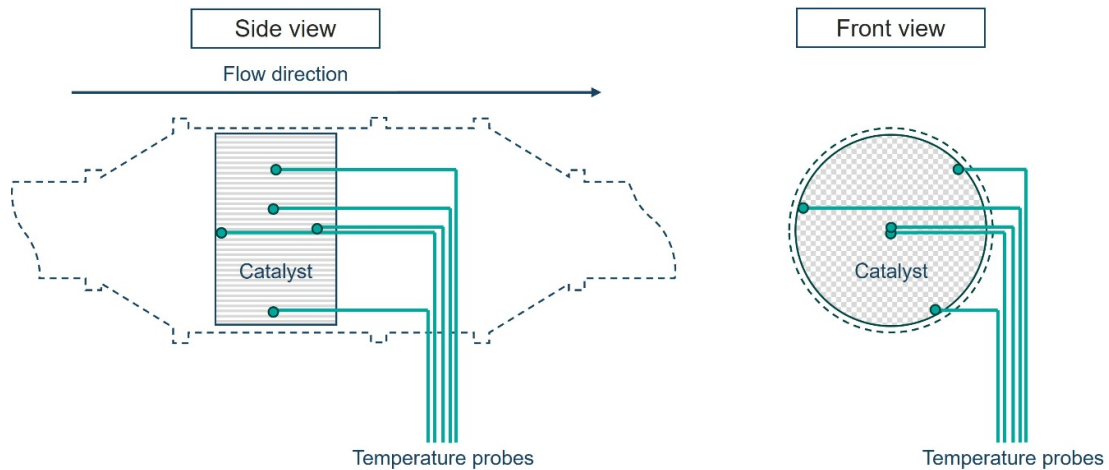


Figure 6: Catalyst temperature locations

2.2.2 Urea injection system

The urea injection system is needed to supply the ammonia that is necessary for the reduction of NO_x emissions in commercial SCR systems. The system built for the test cell consists of a urea injector from a typical diesel passenger car mounted in a sampling pipe with mixing vanes, also from a commercial light duty vehicle. A pressurized tank is used to create the driving pressure for the urea injector. The tank is pressurized by a compressed air line that is connected to the top of the tank. While the pressure can be varied, it was decided to keep the pressure fixed at a relatively high (for the system) pressure of 5 bar. The assumption is that if the high pressure does not need to be compensated for by using too short injector opening durations, a higher pressure would lead to a finer spray and better mixing. The injector is driven by a signal, generated by a pulse generator, that is fed to a switched 12-volt power supply. By varying the pulse width and frequency, the injected amount of urea can be varied. The layout of the urea tank, line and injector are shown in Figure 7:



Figure 7: Urea tank, line to injector and urea injector

The urea solution is injected downstream of the oxidising catalyst, into the bent mixing section that is wrapped in insulating material, visible in the centre of the exhaust system in Figure 4, and indicated in Figure 5. The mixing is used to ensure the even distribution of ammonia in the exhaust gas, before it enters the SCR catalyst.

The system was calibrated with urea-water solution for several injection frequencies and injection durations as well as different injection pressures. At a fixed injection pressure, a linear relationship with the injected amount and the duty cycle of the pulsed control signal was observed. The results were also found to be highly repeatable. Data from the verification tests of the urea system is available in appendix 1.

2.2.3 Temperature probes

The catalysts were fitted with several thermocouples to monitor the temperature at the front and rear of the catalyst, as well as with three probes around the circumference. As the oxidation in the oxidising catalyst and the reduction in the SCR catalyst occurs, a relative temperature increase should be possible to measure. Difficulties may however arise due to the heat loss that will take place between the catalyst and the environment. The temperatures were logged continuously over the time the engine was run.

2.3 Measurement Equipment

Several key measurement instruments have been utilised in the experiments that have been run, in addition to more conventional emission measurement equipment, and is described below.

2.3.1 AVL AMA i60

An AVL i60 system was used to measure the NO, NO_x, CO, CO₂, hydrocarbon emissions and oxygen content in the exhaust gases upstream of the oxidising catalyst, but downstream of the buffer tank. The exhaust fed to the system is divided into two streams, where one is fed to a chemiluminescence detector (CLD), that measures NO and NO_x, as well as the flame ionisation detector (FID) that measures the hydrocarbon emissions. The other exhaust stream is fed through a cooler, that also dries the exhaust, before being fed to a paramagnetic oxygen detector (PMD) and a non-dispersive infrared detector (NDIR), used to measure CO and CO₂.

The position of the measuring probe would allow the system to measure engine out emissions. The AVL system is also connected to the engine dyno and engine controls through AVL Puma. However, this system cannot measure continuously but will only provide time resolved emission and dyno data for roughly 90 seconds per measurement. The oxygen content in the exhaust is only measured here, as the FTIR cannot measure any diatomic homonuclear molecules, such as O₂.

2.3.2 IAG FTIR

An IAG Versa 06 FTIR was used for measurement of pollutant species in the exhaust gases. The FTIR provides the benefit of being able to measure multiple gases at once, most importantly NH₃ and N₂O slip after the SCR catalyst. The system can use two sampling lines but can only use one of them at a time. However, it still enabled the system to be switched from a position downstream of the oxidising catalyst, but upstream of the urea injector. This position will be referred to as sampling point 1 (SP1). Sampling point 2 (SP2) was connected downstream of the SCR. The FTIR also allows continuous measurements at a sampling rate of 2 Hz during long periods of time.

At the point in time that the experiments in this report were performed, a calibration recipe for hydrogen was not available, and a calibration for wet exhaust gases for compressed natural gas was used. The emission of nitrogen oxide species was verified by the AMA i60 and showed good agreement. The FTIR was thus deemed accurate enough for the results to be valid.

2.3.3 Cambustion DMS 500 Mk II

Particle measurements were done using a DMS 500 Mk II fast particle analyser from Cambustion. The system uses a controlled corona discharge to charge incoming particles and measures their charge to aerodynamic drag ratio by detecting where the charged particle lands in the classifier. The result is particle size distribution, as opposed to a particle mass or soot number. One benefit of this, apart from the size information is that the system has a very short response time and thus shows transient behaviours well. The downside is that the mass of the particles needs to be estimated, instead of measured directly. The particle emissions were sampled upstream of the oxidising catalyst, but downstream of the engines exhaust buffer tank and back pressure valve. No catalytic stripper or drier of the exhaust was used, which may cause oil droplets to condense and be registered as particles.

The exhaust temperature was kept high enough, and the instrument is fed through a heated sampling line, kept at a temperature well over the boiling point of water. The sampled gases are diluted by a factor 6 in a cyclone at the sampling point, before reaching the instrument, further lowering the water content in the gases fed through the analyser. In the analyser, the pressure is reduced further. The low pressure and high temperature mean that the water in the exhaust gas will be in gaseous state and not register as particles.

A summary of the measurement instruments used is presented in Table 2.

Table 2: Summary of measurement instruments.

Device	Species Measured	Measuring principle	Range	Unit	Error	Error definition
IAG FITR	NO	FTIR	-	ppm	± 3 %	Relative
	NO ₂		-	ppm	± 3 %	Relative
	N ₂ O		-	ppm	± 3 %	Relative
	NH ₃		-	ppm	± 3 %	Relative
	Formic acid		-	ppm	± 3 %	Relative
	Formaldehyde		-	ppm	± 3 %	Relative
	CO		-	ppm	± 3 %	Relative
	CO ₂		-	%	± 3 %	Relative
AVL AM i60	NO	CLD	10000 ppm	ppm	± 2 %	Estimated
	NO _x		10000 ppm	ppm	± 2 %	Estimated
	O ₂	PMD	-	%	± 1.8 %	Estimated
	CO ₂	NDIR	20%	%	± 1.8 %	Estimated
	CO ₂ (low)		6%	%	± 1.8 %	Estimated
	CO		10%	%	± 1.8 %	Estimated
	CO (low)		5000 ppm	ppm	± 1.8 %	Estimated
	THC	FID	900 ppm	ppm (C3)	± 0.5%	Relative
Cambustion DMS 500	PN		0-300	nm	± 5%	Relative
			300-1000	nm	± 10%	Relative

The error given in the table for the AVL instruments is a combination of multiple sources of error. For the NO and NO_x instruments, these errors are the relative errors of quenching 1%, noise 1 %, linearity 1%, reproducibility 0.5 % of full range, drift 1%/24h. The quenching error source is unique to the CLD in the system, as it measures wet exhaust gases, however, the analyser used is the super low quench version to minimise this error. The other instruments do not measure wet emissions, and the error sources for these are given as noise 1 %, linearity 1%, reproducibility 0.5 % of full range, drift

1%/24h. The estimated total error was calculated assuming that the error sources are independent.

2.4 Design of Experiments

2.4.1 Design

The goal of the experiments escribed in this report was to investigate how the unique properties of a hydrogen internal combustion engine influences components in an exhaust aftertreatment system. These unique properties are mainly the high concentration of water in the exhaust that will be significantly higher than in a conventional diesel engine, but also the absence of hydrocarbons and carbon dioxide. The objective was to investigate the effect on an both an oxidising catalyst and an SCR system. For the oxidising catalyst experiments, a design of experiments (DoE) approach was used to investigate the engine out emissions as well as the properties of the oxidising catalyst, which has faster time response than the SCR catalyst. This means that more experimental points could be run, and the results could be repeated. Data from the DoE would then be used to select a few points for more in-depth investigation of the SCR system, as these experiments would be more time consuming, due to the ammonia storage capacity of the SCR catalyst and associated longer time to reach stable conversion.

For the catalysts, the key parameters that is expected to impact their efficiency is the total NO_x levels, the space velocity and the water content. The temperature is also of interest but is included as an uncontrolled factor in the analysis. An overview of the factors and their predicted effects are given in Table 3:

Table 3: Design of experiment primary factors (rows) and their predicted influence on secondary factors (columns).

Parameter	NO _x	Space velocity	Water content	Temperature (uncontrolled)
Engine Speed	→	↑	→	↑
Intake Pressure	↓	↑	↓	↓
MFB 50	↑	→	→	↓

In the design, the parameters that has the biggest predictable effect on the emissions was chosen as the factors. The desire to ensure maximum separation between measurement point in the narrow design space, led to the selection of a face centred cubic design with engine speed, intake pressure and combustion phasing as the primary factors.

The air-fuel ratio is controlled by changing the intake pressure, as the fuel injected per cycle was kept constant. It has a strong influence on the engine out NO_x emissions, as well as on the water content and temperature of the exhaust gases. Ignition timing was varied to change the combustion phasing, defined as the point where half of the injected fuel mass fraction have burned (MFB50). Early timing raises the in-cylinder temperature and thus NO_x emissions without affecting the water content or the space velocity in the exhaust gases. While the start of injection (SOI) timing can impact NO_x emissions, the

impact is less predictable and the range of injection timings that could be run while satisfying the conditions that SOI was after IVC was limited, and SOI was thus excluded from the DoE, as varying the combustion phasing would have a similar, but more predictable effect on the engine out NO_x emissions. Finally, the engine speed was included as a factor to be able to vary the space velocity of the exhaust gases through the catalysts independently of the air-fuel ratio and thus possibly avoid confounding between water content, NO_x emissions and space velocity. In practice, the air-fuel ratio was controlled by changing the intake pressure between fixed levels.

The settings for each operating point along with its number are given in Table 4:

Table 4: Design of experiments, test points and factors.

Experiment #	Speed [RPM]	Intake Pressure [mbar]	MFB50 [°ATDC]
1	1400	1300	7,0
2	1400	1300	2,0
3	1400	1180	4,5
4	1400	1060	7,0
5	1275	1300	4,5
6	1275	1180	7,0
7	1150	1300	7,0
8	1275	1180	4,5
9	1400	1060	2,0
10	1275	1180	2,0
11	1150	1300	2,0
12	1275	1060	4,5
13	1150	1180	4,5
14	1150	1060	7,0
15	1150	1060	2,0

The complete DoE was repeated three times. Point 1 was used as a reference to check that the engine's condition was ok before the runs and was repeated every time the engine was started. and was repeated multiple times, including at least once every time the engine was started. Thus, the centre point was not repeated more than once per run of the DoE, and the reference point was used to check for repeatability of the experimental setup. The order of the points was randomised. Naturally, this allowed small variations in catalyst temperature for each point, depending on the history of the specific run order for the day, which is why the catalyst temperature, while important for the function of the catalysts, are not considered a controlled variable.

2.5 SCR Evaluation

The SCR system has a slow time response compared to the engine and DOC. Testing is thus more time-consuming than just measuring the engine out emissions.

From the design of experiments, three points were chosen to gain insight into the performance of the SCR and how it depends on the engine operating characteristics. The first point was chosen to be close to the first point in the DoE, but the spark timing was

advanced slightly to increase the engine out NO_x, as higher levels of NO_x would make the relative error in the measurements less significant. A second operating point was chosen, at a similar engine speed but at lower intake pressure, to increase the amount of water and NO_x in the in the exhaust gases. Finally, the third point was chosen to be like the first SCR point, but at a lower engine speed. This would create a gas composition like the first point, but at a space velocity close to that of the second point, to be able to separate the factors as much as possible in three experiments. Each operating point was operated with a target ammonia to NO_x ratio (ANR) of 0.8 and 1.2. Between the periods with an active SCR, the engine was allowed to run until the ammonia slip and NO_x conversion was zero again, indicating an empty catalyst and equal starting conditions for all six periods with active SCR. A summary of the points, including the corresponding points in the DoE, is given in Table 5:

Table 5: Summary of SCR test points.

SCR Point	DoE Point	Speed [RPM]	Intake Pressure [mbar]	MFB50 [°ATDC]	Target ANR
1	2	1400	1300	2,0	0.8, 1.2
2	4	1400	1060	7,0	0.8, 1.2
3	11	1150	1300	2,0	0.8, 1.2

During the SCR runs the FTIR sampling point was switched between a position downstream of the SCR catalyst and a position upstream of the SCR and the urea mixing section but downstream of the oxidising catalyst. At intervals, the AMA i60 was used to capture the engine out emissions, which would allow comparison with the engine out emissions.

As the AMA i60 chemiluminescence NO_x detector and the FTIR only showed a difference in a few ppm between measurements, this approach was deemed accurate enough, despite the difference in operating principle of the measurement instruments.

The runs will later be referred to as, e.g. SCR 2 high, indicating that it is SCR point 2, for the high ANR.

3 Results

3.1 Engine-Out Emissions & Oxidising Catalyst Performance

The engine-out emissions that are the most concerning for a hydrogen ICE is the nitrogen oxides. These were measured upstream and downstream of the oxidising catalyst. Figure 8 shows the estimated level due to a model fit, and includes the measure points indicated by the circles, where the fill colour indicates the total NO_x level. As expected, the NO_x emission decreases with increased intake pressure, however, the relative impact of the combustion phasing is considerably smaller, when compared to the influence of the intake pressure, and thus the air-fuel ratio. This presents a problem for the following SCR trials, as well as for the evaluation of the impact of the unique properties of a hydrogen engine on the efficiency of a conventional EATS, as the impact of water content, which depends on ten air/fuel ratio, is highly confounded with the impact of NO_x concentration. To a smaller degree it also influences the temperature, which increases as the air/fuel ratio decreases. The space velocity can still be varied independently of the water and NO_x content, however.

The total NO_x levels followed the predicted trend, with early timing increasing the emissions of NO_x , and richer mixtures, corresponding to lower intake pressures, resulting in drastically increased NO_x emissions.

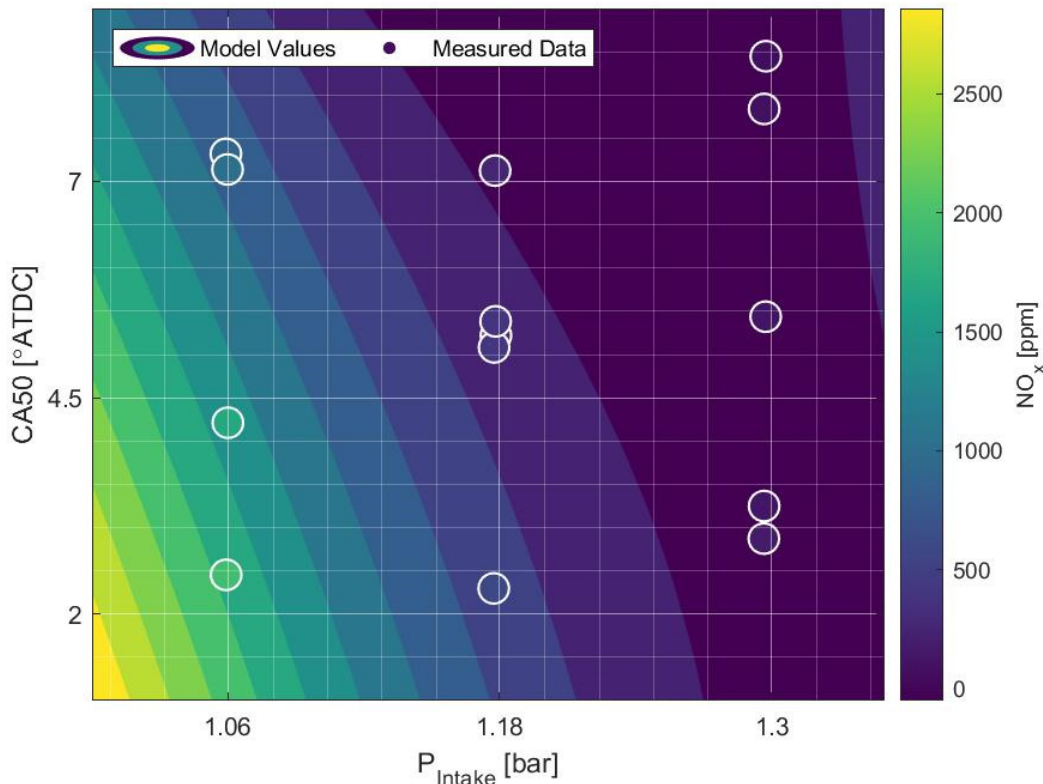


Figure 8: Engine out NO_x emissions. Engine speed was found to have negligible impact on the concentration.

In addition to the total levels, the ratio between NO_2 and total NO_x is of interest as this highly influences the operation of an SCR system. The engine out emission was found to vary with the total NO_x level, however the NO_x levels are highly correlated with the water content in the exhaust gases, and it is difficult to determine whether the water levels or the NO_x levels are crucial. Fitting a linear regression model to the NO_x emissions does however show a better fit than a model fitted to the water content, with a higher R^2 value for the NO_x emissions. Confounding of the variables makes determining which is the determining factor impossible from the data alone. The NO_2/NO_x ratio and the fitted line are shown in Figure 9:

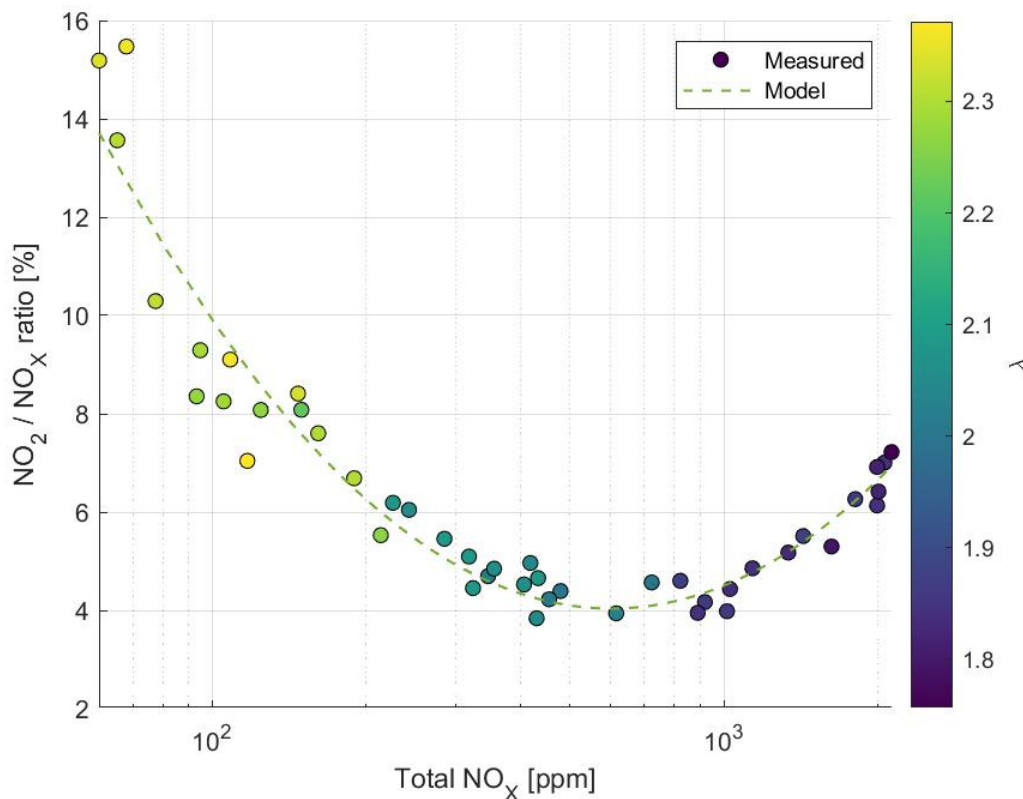


Figure 9: Engine out NO_2/NO_x ratio

Also shown in the figure is the lambda for the measurement points from the three repeats of the DoE. The gradual decrease in λ -values as the NO_x emission increase shows the strong correlation between λ , and thus water content, and NO_x content with NO_2/NO_x in the engine out exhaust.

While the engine out NO_2 to NO_x ratio can be estimated from the total NO_x alone, the downstream NO_2 to NO_x ratio shows more complex behaviour. The ratio downstream of the oxidising catalyst is shown in Figure 10:

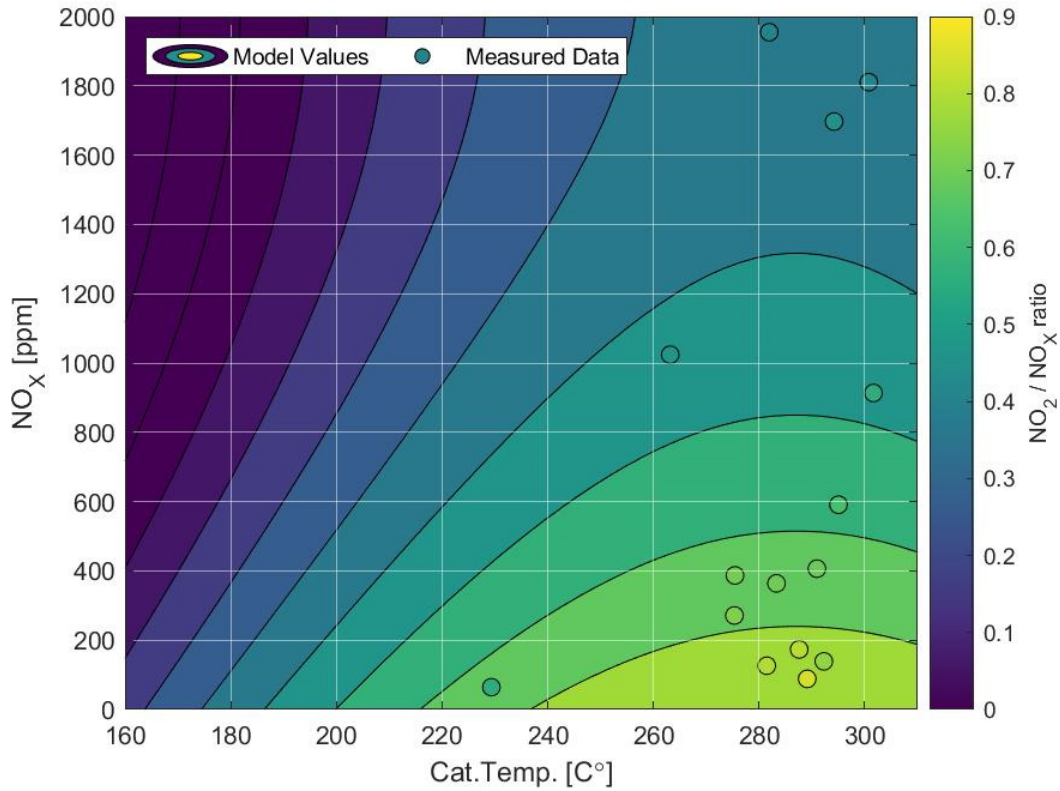


Figure 10: NO_2 to NO_x ratio downstream of the oxidising catalyst for the DoE

At low NO_x concentrations, the NO_2/NO_x ratio is consistently high. This correlation between the ratio and the total NO_x concentration will present a challenge for the SCR trials, as the NO_2/NO_x is crucial for high conversion. If it is higher than 0.5, the reduction of NO_2 will be forced to occur through the slow reaction pathway. However, the total NO_x is strongly dependent on the air/fuel ratio, which also directly determines the water concentration in the exhaust gases. This requires the difference over time at an operating point to be significant compared to the variations within an operating point. The issues with the variation of NO_x emissions while operating close to steady state will be covered more deeply in section 3.2

The influence of total NO_x on the NO_2/NO_x ratio downstream of the oxidising catalyst, and the correlation with total water content means that unless the NO_x concentration is stable at each operating point, the relative difference in concentration due to combustion phasing will be small in practice. This presents a challenge for the evaluation of the SCR performance later and is one of the key reasons conclusions regarding the engine operating parameters from the DoE cannot be drawn, and that more experiments are needed once a method for decoupling some of these effects is developed.

The temperature dependence at low temperatures is illustrated in Figure 11, where the NO_2/NO_x ratio for the first start of the engine, with a cold EATS, is shown for four repeated starts, at load point 1 in Table 4. As the temperature of the exhaust system at

the time of engine start is slightly different depending on previous activity, zero minutes is defined as the point where the oxidising catalyst has first reached a temperature of 125 °C.

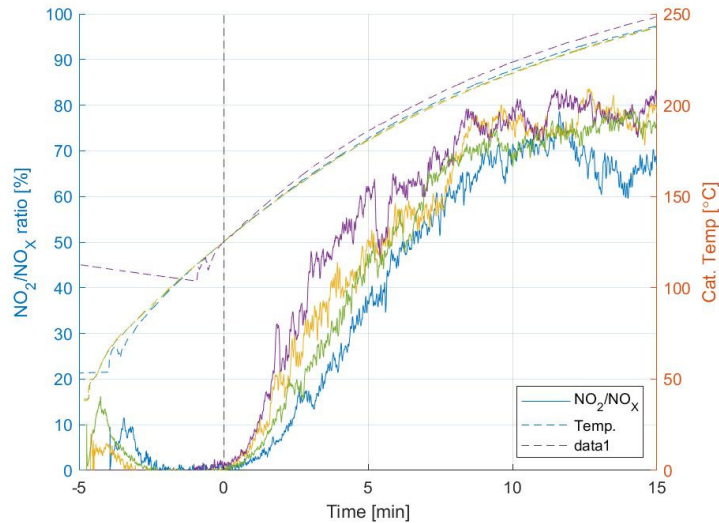


Figure 11: NO_2/NO_x ratio downstream of the oxidising catalyst at engine start

The dashed lines in the figure indicate shows the temperature of the catalyst, while the solid line shows the NO_2 to NO_x ratio downstream of the catalyst. After 200 °C, the curves flatten, indicating that peak NO oxidation occurs at these temperatures. As the catalysts heat up further, it is expected that the NO_2 to NO_x ratio decreases, as the thermal equilibrium at higher temperature favours higher NO levels.

3.2 SCR Catalyst Performance

The SCR catalyst shows a large time dependence in its response, due to the ammonia storage capacity and the time it takes to reach equilibrium. Some studies have shown that even after 4.5 hours, an SCR system at comparable conditions may not have reached steady state operation [12]. A compromise with regards to urea and hydrogen consumption led to the choice of a time of 60 minutes per operating point in Table 5 for the SCR system, as this was deemed sufficient for the system to reach somewhat steady conversion, if not complete steady state conditions. Case 2 with high ANR will be used to illustrate the behaviour of the system, but data from the other runs are presented in Appendix 3.

For case 2 with a target ANR at 1.2, the reduction in NO_x for the later points, when conditions in the SCR have stabilised, seems to be around 98%. The continuous and intermittent measurement measured emissions are shown in Figure 12.

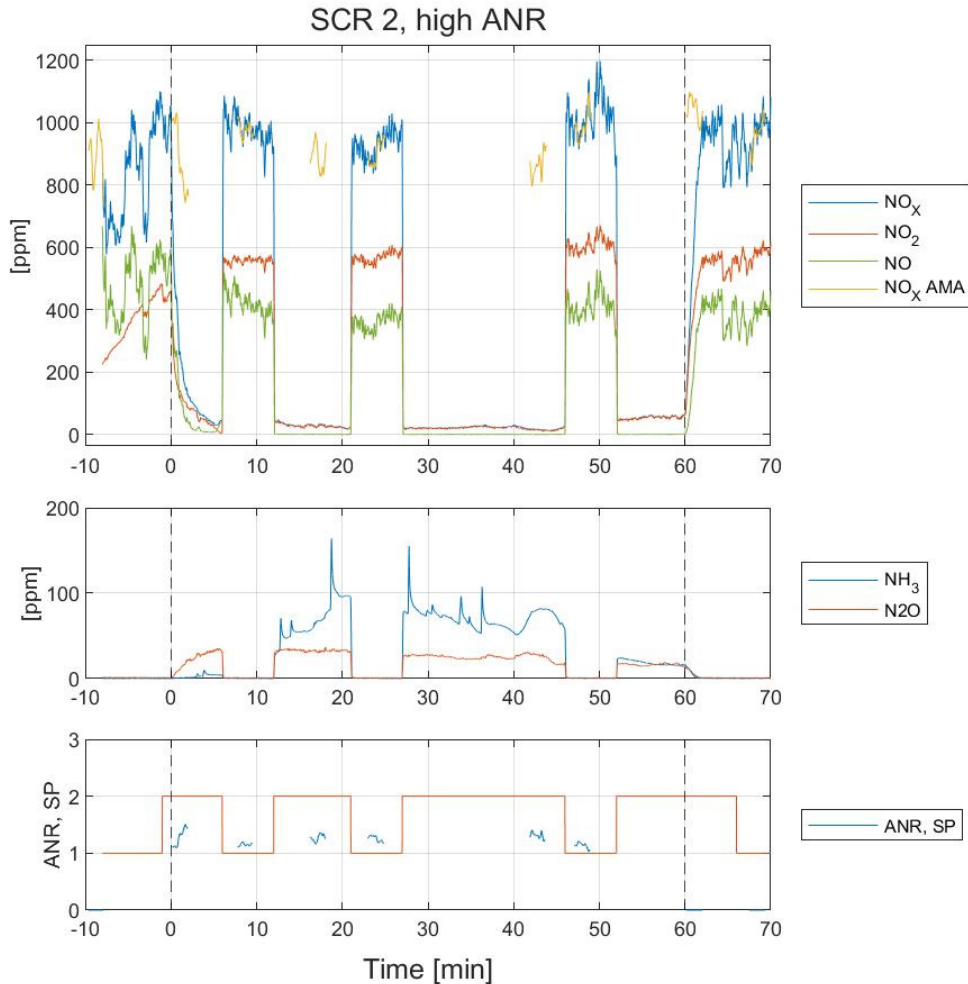


Figure 12: Detailed results from SCR case 2, high ANR target at 1.2.

The top graph shows nitrogen oxide species measured by the FTIR and AMA i60. The middle graph shows the ammonia slip and N₂O generation, while the bottom graph indicates the sampling point of the FTIR system and the calculated ANR based on the engine out NO_x levels measured by the AMA i60 CLD.

The NO_x reduction starts slowly and reaches somewhat steady levels at around 20 minutes into the run. The NO_x emissions, in blue in the top graph, are shown to be slightly unsteady, which in turn made urea dosing difficult. The slightly lower emissions of NO_x at around 20 minutes, also contributes to a period of very high NH₃ slip, but as the NO_x emissions increase near the end of the period, the NH₃ slip decreases. There is also a considerable generation of N₂O in the catalyst at these conditions, possibly due to the excess amount of NH₃ injected and high NO₂ to NO_x ratio.

The results from the low ANR runs, available in Appendix 3, confirm that at low ANR, there is very little slip of NH₃ or generation of N₂O. The engine operating was however too unstable, and the emissions varied too much for statistical models for the ammonia

slip and N_2O generation to be modelled, partly caused by the lack of upstream gas composition at the time of measurements, apart from the estimated NO_2 to NO_x ratio.

Generally, when there is no NH_3 available in excess to the NH_3 required to reduce the NO_x , it appears that there is very little N_2O generated. However, for the cases with a high ANR, and excess NH_3 and N_2O is generated. This highlights that the key to efficient SCR systems is accurate urea dosing, which in turn would require either sensors or a good model of the engine out emissions in real world, transient operation. While the focus in this paper is on steady state operation, the variations over time of NO_x variations in the current engine makes this slightly difficult.

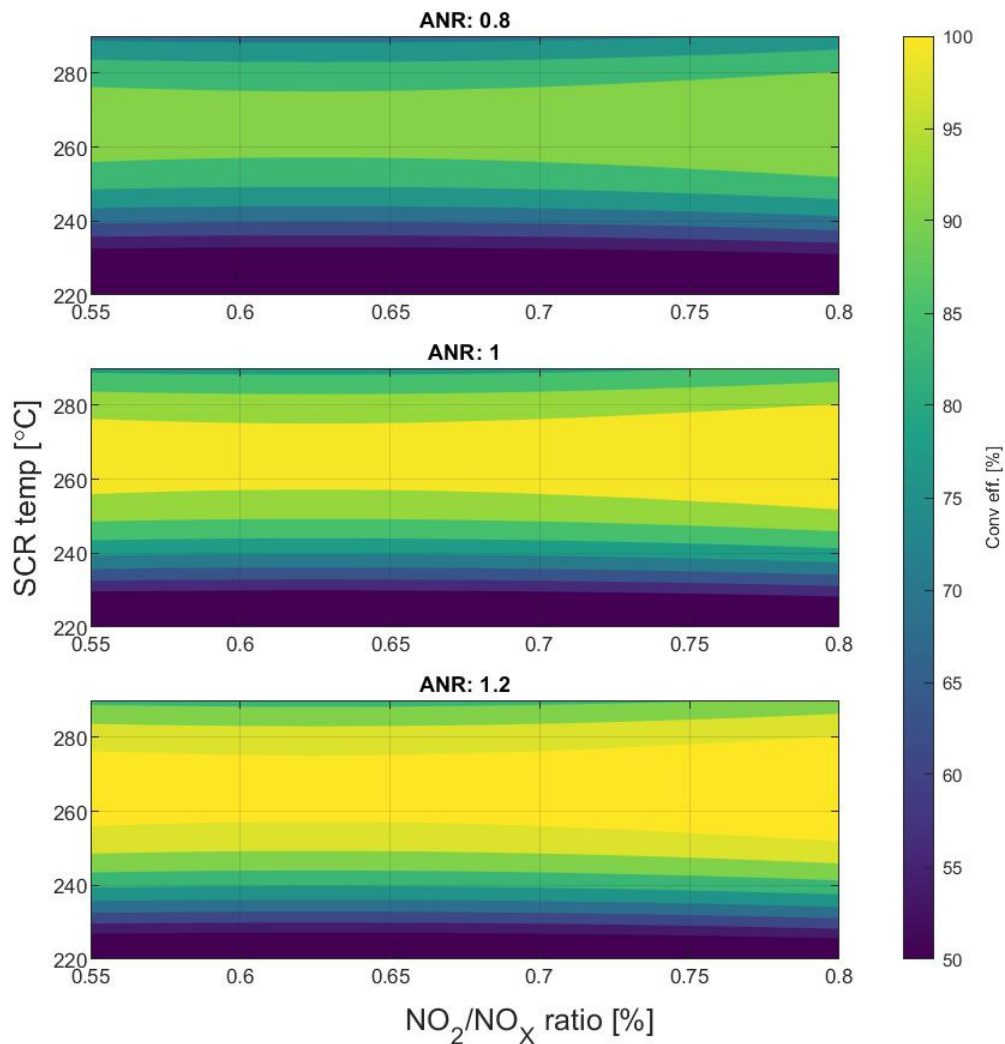


Figure 13: NO reduction efficiency of the SCR catalyst.

Since the ratio of NO_2 to NO_x could not be measured simultaneously with the emissions downstream of the SCR system, as the FTIR system only has one sampling probe, the model that was illustrated in Figure 10 was used to estimate the ratio upstream of the SCR catalyst. The results showed that the ratio has some impact on the conversion

efficiency, with slightly higher conversion at higher ratios. This could be caused by the NO being consumed in the fast SCR reactions, until it is depleted. The cause of the decrease in the model efficiency at high temperatures matches those observed for both the NO₂ reduction efficiency and the NO_x reduction.

The NO₂ conversion on the other hand showed lower conversion efficiencies in general. A likely reason for this is that all the points were operated at NO₂ to NO_x ratios over the optimal 50%, which causes some of the NO₂ to be reduced through the slow SCR reaction.

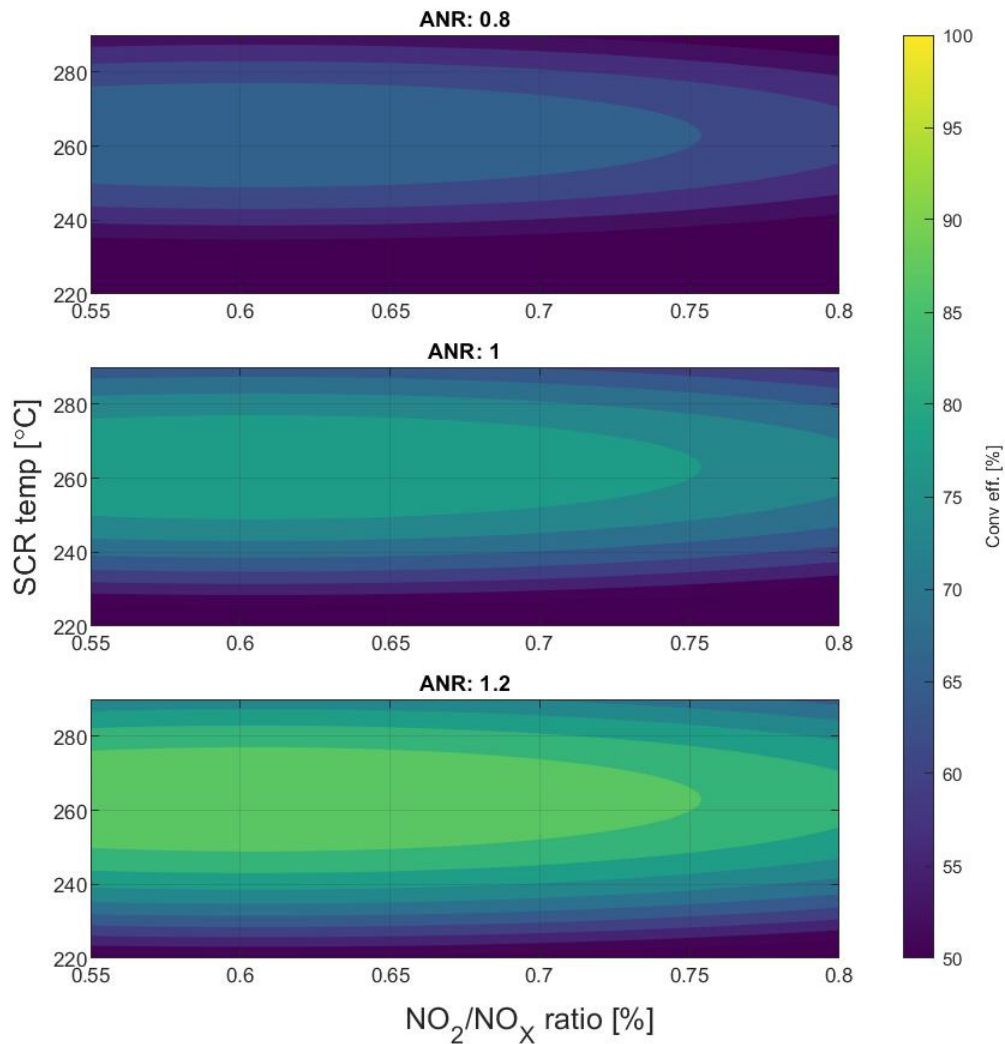


Figure 14: NO₂ reduction efficiency of the SCR catalyst.

The total NO_x reduction efficiency on the other hand showed no statistically significant dependence on the upstream NO₂ to NO_x ratio. Rather, the total NO_x ratio was influential in determining the efficiency. The concentration of NO_x and water are however so closely correlated, that it is impossible from the data to draw conclusions. Inclusion of

both factors in the regression model leads to poorly conditioned dataset, with a condition number over 100. This is one of the main drivers behind the installation of a heated, uncoated catalyst and the water injection system, as independent control of water concentration and the ability to increase the temperature of the exhaust gases will lead to better data for a deeper understanding of the influence of water at more realistic temperatures. The total NO_x reduction efficiency is shown in Figure 15:

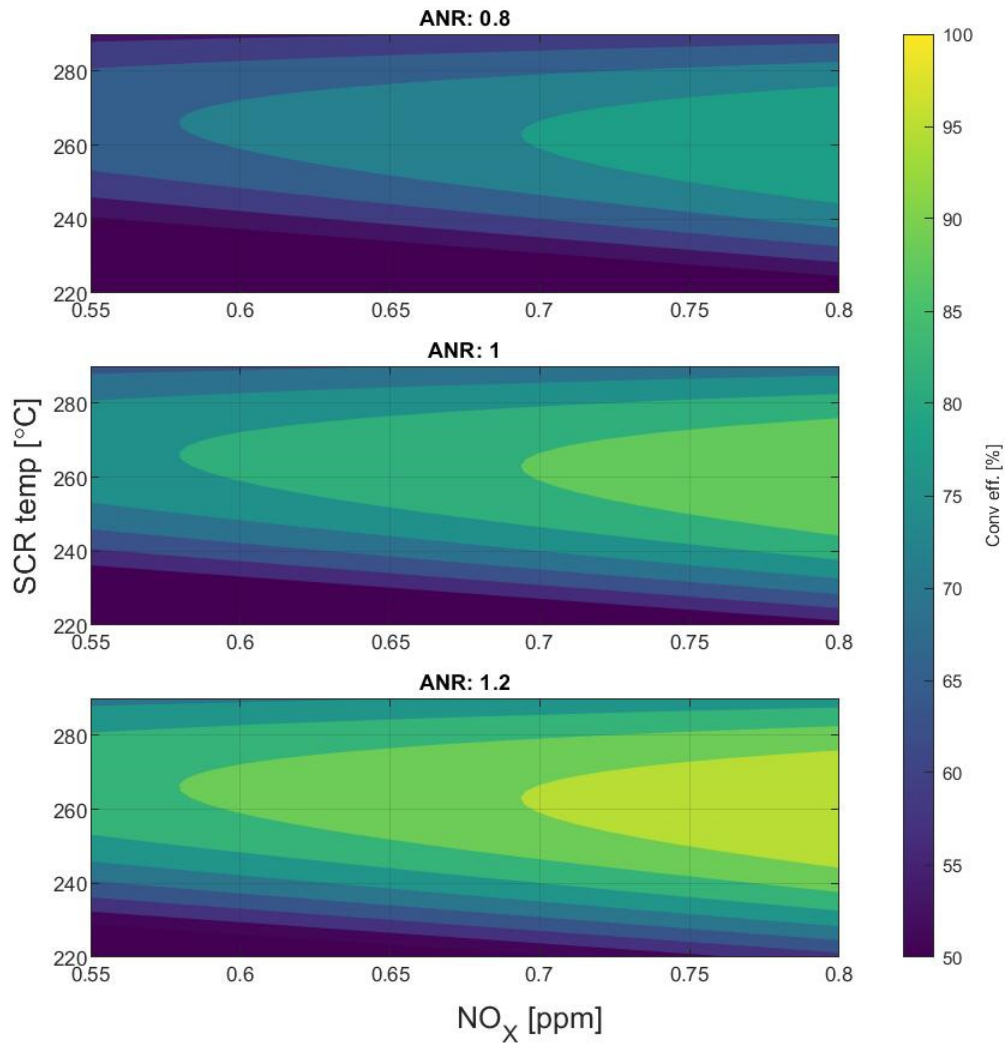


Figure 15: NO_x reduction efficiency of the SCR system

Somewhat surprisingly, the conversion efficiency of the SCR catalyst increased with increased NO emission. In the future, use of heater to increase temperature of the catalyst would give more insight into effect even higher temperatures have on the efficiency, as a catalyst temperature of only 260 °C is considerably lower than the engine out exhaust temperature, which in most of the tests have been between 400 and 500 °C. The large buffer tank led to high heat losses in the experimental setup, something that needs to be compensated for if more realistic catalyst conditions is to be achieved.

3.2.1 PN from Design of Experiments

Particle emissions were measured for the whole range of experiments performed. The results show large variations over times, which makes conclusions regarding the effects of the parameter changes over the design of experiments inconclusive. The results of these measurements are shown in Figure 16. The figure contains data from the first two repeats of all the points from the DoE, and it is clearly seen that the variation for the same measurement point is at least on a similar scale as the differences between the operating points. The differences in particle numbers seen between DoE A and DoE B shows that it is impossible to draw any conclusions regarding the effect of the operating characteristics on the particle emissions.

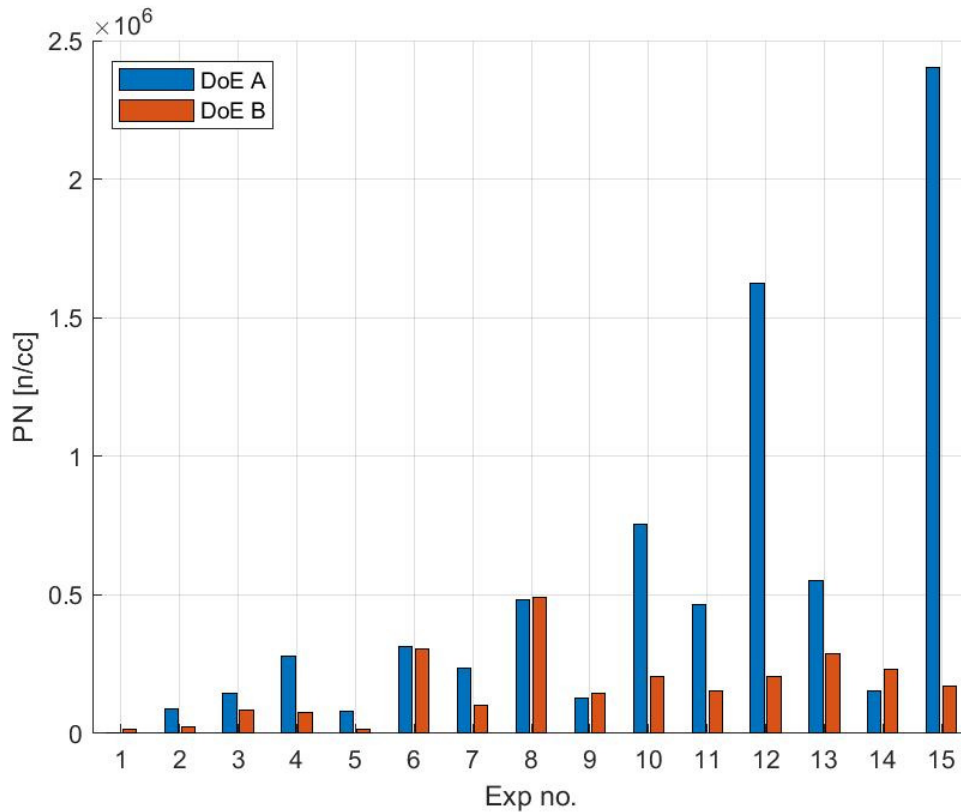


Figure 16: Engine out PN emissions from the DoE.

While the particle emissions were not repeatable between different load points, it was observed that the particle emission increased rapidly after the first fired cycles each time the engine was started, before decreasing to low levels. Figure 17 shows the emission at engine start. It can be observed that after a few minutes of operation the emissions are below the motored levels for all engine starts. This is most likely caused by the DMS measuring oil droplets as well, and as the temperature of the cylinder walls and engine oil increases, more of the oil is burned, and converted into CO₂ or CO, instead of escaping as small droplets that can be picked up by the DMS as particles.

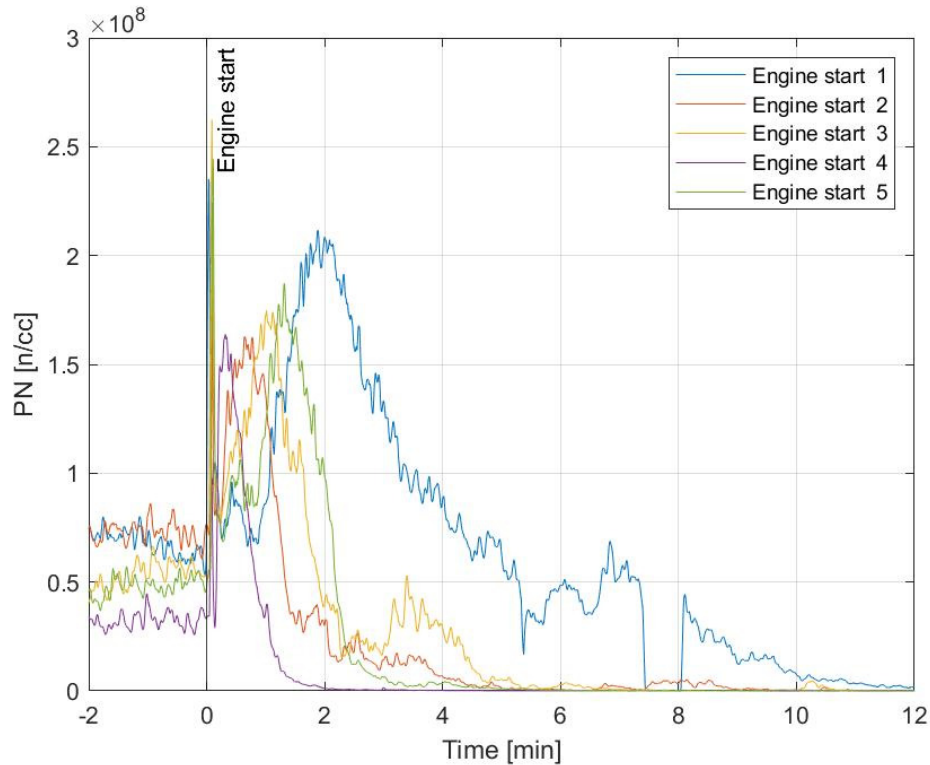


Figure 17: Engine out particle emissions at engine start.

The same trend can be observed in all the engine starts, but the absolute levels and the duration for which they are high varies. A possible explanation for some of the variations may be the length of time the engine has been stopped, and the amount of oil that has been collected in the cylinder. In Figure 17, the highest number of particles is for the engine start 1, which also has among the highest emissions during motored operation, possibly indicating a larger amount of accumulated oil in the combustion chamber.

Focusing on the size distribution for first engine start, a trend is observed where the particle numbers remain almost constant for period, before a gradual increase in total PN. However, the size of the particles follows a different trend. At first, while the numbers remain the same, the size gradually increases, before diminishing again as the particle numbers reach their peak values. This is illustrated in Figure 18 :

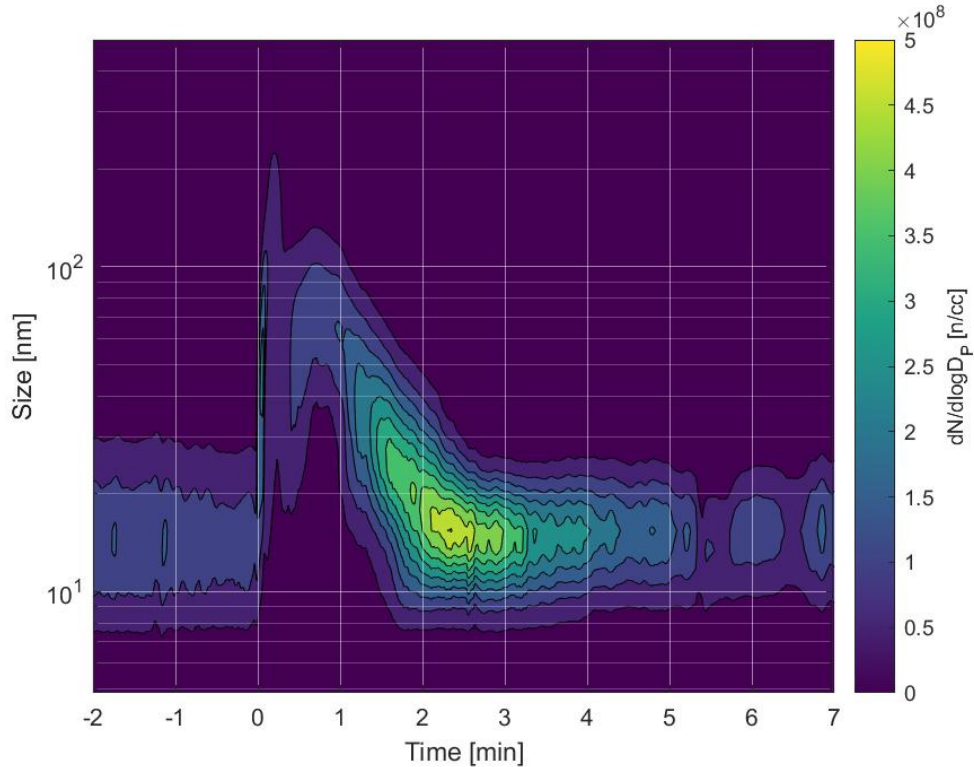


Figure 18: Size and number of particles at engine start 1. Engine starts at 0 seconds.

Engine start 1 was chosen for illustrative purposes, as the trend looks similar in all points, but engine start 1 had the highest particle numbers for the longest duration, and the trends are clearer. As the engine is first started, the particle size is large, indicating that the particles are large, but relatively few, as the numbers are reasonably low. The numbers peak at around 2.5 minutes after the engine is started, at which point the size of the particles are small. This also shows that larger particles are almost non-existent in the exhaust flow after approximately 2 minutes.

This most likely coincides with higher in-cylinder temperature, and more complete combustion of engine oil. As the accumulated engine oil is burned off, the emissions are reduced to levels that are below those of motoring the engine, as seen in Figure 19, which shows the total PN over time in the top graph, and the size distributions at a few instances, namely motored operation before the first firing of the engine, one point where the size of the particles reach their peak. This is followed by a point where the numbers peak, and a point 15 minutes later, where the levels have reduced to a fraction of what they were before the engine was even started.

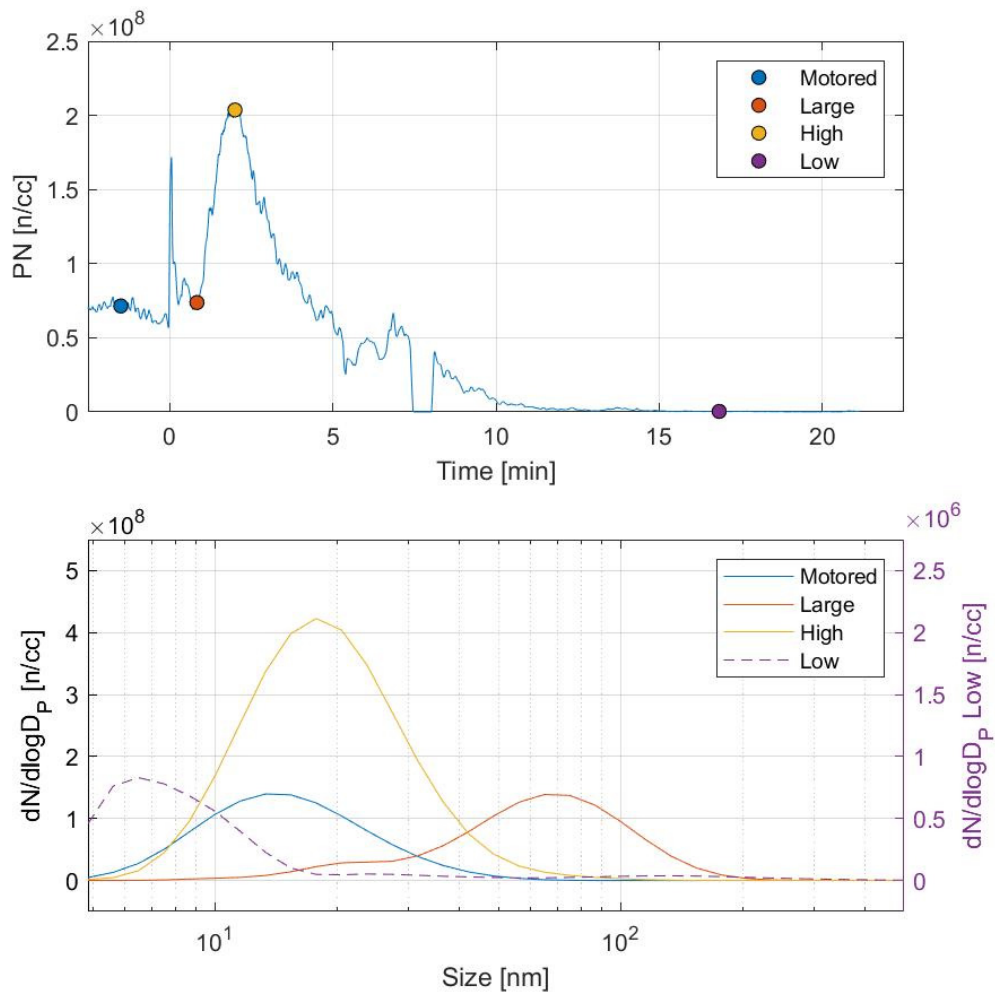


Figure 19: Size distributions at four points after engine start 1.

The “low” point in the graph, indicated by a dashed line, is reading levels around 1 % of the motored level, and has its own y-axis, as the size distribution would be impossible to see in the figure otherwise. While the sizes of the particles at motored conditions and at their peak was similar, the mean particle size at the low point is even smaller.

4 Discussion

4.1 Limitations

4.1.1 Limiting Factors of DoE

The engine used in the lab was limited in the range of operating points that could be run at the beginning of the experimental campaign. Maximum load was limited by prevalent pre-ignitions to around 7 bar IMEP, while the maximum engine speed was limited to 1400 rpm, at which speed random cuts in the communication with the ECU would occur, possibly due to limited bandwidth. Severe combustion instability at low engine speeds limited the engine to speeds over 1150 rpm.

Further constraints were imposed by less severe, but still important factors. In trying to keep the load constant (and as high as possible) the minimum air/fuel ratio that could be reached without imposing high pumping losses was limited by the exhaust back pressure. The main reasoning for the avoidance of throttled operation at this load was that throttling would impose an unnecessary (and obvious) efficiency penalty, and this mode of operation would be avoided.

The maximum advance of the spark timing was limited such that the earliest combustion phasing was 2° ATDC, to ensure that all operating points could be run with a small margin to knock.

The NO_x emissions was also a limiting factor. As combustion phasing was retarded and the intake and exhaust pressure were increased, the NO_x emissions were reduced. Any later combustion phasing or higher intake pressures would result in near-zero NO_x emissions which, while desirable, renders investigation of the effect of e.g. water content in the exhaust gases and their impact on catalyst efficiency impossible.

4.1.2 Practical considerations

The unsteady fuel flow, and the associated unsteady levels of NO_x in the exhaust made separating the effects of NO_x and water difficult in practice. If the engine-out emissions would have been stable, the difference in total NO_x due to the combustion phasing would still have been smaller than the impact on NO_x of the air/fuel ratio, however, changing the NO_x emissions with at least a factor 2 at steady water levels and space velocities should have been possible, and was in general achieved in the DoE runs. The impact on ANR and inability to measure all emissions continuously leads difficulties in estimating the stored ammonia, as there is no way of knowing for certain what the ANR was in the time leading up to a measurement.

The variations also introduced an additional difficulty in that time synchronization of data turns into a potentially severe source of error. Measurement instruments located in different locations in the test cell, with different lengths of connecting hoses and gas flow rates, as well as different response times, introduces additional errors compared to ideal steady state testing. Operations such as calculating catalyst conversion or ANR can

be subject to error if, e.g. the NO_x levels suddenly drop during a measurement and the instruments are not synchronised. In the DoE, when measuring over the oxidising catalyst, the total level of NO_x is not expected to change, and this can be used to synchronise the response in time. During the SCR runs, this is more of an issue, as there is no variable that is not expected to change that can be measured with the AVL system and the FTIR simultaneously.

Improvements in the test setup, and the planned inclusion of a heated, uncoated catalyst brick and water injection system, should allow some of these issues to be overcome, as independent control of water and temperatures become possible.

5 Conclusions

The experiments have confirmed that the engine-out NO_x levels are dependent on the air-fuel ratio and combustion phasing, as expected, with minimal impact from engine speed.

The oxidising catalyst shows conversion of NO into NO₂. The key factors that influence the downstream NO₂/NO_x ratio is found to be the total NO_x level, water content and temperature of the oxidising catalyst, where an increase in temperature increases the downstream NO₂ levels. Both high total NO_x levels and high water concentrations correlate negatively with the NO₂/NO_x ratio. The ratios observed were above the 50 % that is optimal for achieving the fast SCR reaction.

The key conclusion regarding the performance of the SCR system so far is that with the experimental setup as it is currently configured, there will be no way to differentiate the impact of water concentration and NO_x concentration, due to confounding between variables and unsteady engine operation. There is still a trend shown in the increased reduction of NO_x at higher ANRs, but with the downside and temperature have an impact on the reduction as well. The results have shown that a reduction of NO_x in a conventional SCR system is clearly possible even with a commercially available system, and there is no reason to believe that a DISI hydrogen engine cannot achieve low tailpipe levels.

Development of the experimental setup is needed before the research question can be answered satisfactorily.

References

- [1] C. Bekdemir, E. Doosje, and X. Seykens, "H₂-ICE Technology Options of the Present and the Near Future," 2022, SAE Tech. Paper 2022-01-0472. [Online]. Available: <https://doi.org/10.4271/2022-01-0472>.
- [2] R. Babayev, A. Andersson, A. Serra Dalmau, H. G. Im, and B. Johansson, "Computational comparison of the conventional diesel and hydrogen direct-injection compression-ignition combustion engines," *Fuel*, vol. 307, p. 121909, 2022/01/01/ 2022, doi: <https://doi.org/10.1016/j.fuel.2021.121909>.
- [3] V. Mittal, R. Shah, N. Aragon, and N. Douglas, "A Perspective on the Challenges and Future of Hydrogen Fuel," *SAE International Journal of Sustainable Transportation, Energy, Environment, & Policy*, vol. 3, no. 1, pp. 31--39, oct 2021, doi: <https://doi.org/10.4271/13-03-01-0003>.
- [4] K. K. Rana, S. Natarajan, and S. Jilakara, "Potential of Hydrogen Fuelled IC Engine to Achieve the Future Performance and Emission Norms," 2015. [Online]. Available: <https://doi.org/10.4271/2015-26-0050>.
- [5] S. Sterlepper, M. Fischer, J. Claßen, V. Huth, and S. Pischinger, "Concepts for hydrogen internal combustion engines and their implications on the exhaust gas aftertreatment system," *Energies*, Article vol. 14, no. 23, 2021, Art no. 8166, doi: 10.3390/en14238166.
- [6] S. Verhelst, "Recent progress in the use of hydrogen as a fuel for internal combustion engines," *International Journal of Hydrogen Energy*, vol. 39, no. 2, pp. 1071-1085, 2014/01/13/ 2014, doi: <https://doi.org/10.1016/j.ijhydene.2013.10.102>.
- [7] M. Oikawa, Y. Takagi, Y. Mihara, N. Kawahara, E. Tomita, and K. Naitoh, "Attainment of High Thermal Efficiency and Near-zero Emissions by Optimizing Injected Spray Configuration in Direct Injection Hydrogen Engines," 2019, SAE Tech. Paper 2019-01-2306. [Online]. Available: <https://doi.org/10.4271/2019-01-2306>.
- [8] L.-z. Bao *et al.*, "Development of a turbocharged direct-injection hydrogen engine to achieve clean, efficient, and high-power performance," *Fuel*, vol. 324, p. 124713, 2022/09/15/ 2022, doi: <https://doi.org/10.1016/j.fuel.2022.124713>.
- [9] P. A. Dennis, R. J. Dingli, P. Abbasi Atibeh, H. C. Watson, M. J. Brear, and G. Voice, "Performance of a Port Fuel Injected, Spark Ignition Engine Optimised for Hydrogen Fuel," 2012. [Online]. Available: <https://doi.org/10.4271/2012-01-0654>.
- [10] T. Waldron and J. Brin, "Benefits of a driven-turbo for hydrogen internal combustion engines," in *15th International Conference on Turbochargers and Turbocharging: Proceedings of the 15th International Conference on Turbochargers and Turbocharging (Twickenham, London, 16-17 May 2023)*, 2023, pp. 56-68.
- [11] Ö. Can, S. Stefan, R. Sebastian, E. Helmut, and P. Stefan, "Exhaust gas aftertreatment to minimize NO_x emissions from hydrogen-fueled internal combustion engines," *Applied Energy*, vol. 353, p. 122045, 2024, doi: <https://doi.org/10.1016/j.apenergy.2023.122045>.
- [12] N. Ottinger, Y. Xi, C. Keturakis, and Z. G. Liu, "Impact of Water Vapor on the Performance of a Cu-SSZ-13 Catalyst under Simulated Diesel Exhaust Conditions," *SAE International Journal of Advances and Current Practices in Mobility*, vol. 3, no. 6, pp. 2872--2877, apr 2021, doi: <https://doi.org/10.4271/2021-01-0577>.

Abbreviations

ANR	Ammonia to nitrogen oxides ratio
CLD	Chemiluminescence detector
DI	Direct injection
DoE	Design of experiments
EATS	Exhaust after-treatment system
H ₂ O	Water
ICE	Internal combustion engine
IVC	Intake valve closing
MFB50	50% mass fraction burned
N ₂ O	Dinitrogen monoxide
NDIR	Non-dispersive infra-red
NH ₃	Ammonia
NO	Nitric oxide
NO ₂	Nitrogen dioxide
NO _x	Nitrogen oxides
PMD	Paramagnetic (oxygen) detector
SCR	Selective catalytic reduction
SI	Spark ignition
SOI	Start of injection
SP1	Sampling point 1
SP2	Sampling point 2

Appendix 1: Urea Calibration Data

The urea system was tested by allowing it to run at different injection pressures, injection frequencies and opening durations. The tests were performed with water at first, before a run of experiments with a typical, commercially available, water/urea mixture was used. The test results on pure water are shown in Table 6:

Table 6: Urea/water injector settings and calculated flow rates for pure water.

Measured Values					Calculated Values		
Pressure	Pulse	Time	Weight before	Weight after	Δ Weight	Flowrate	Duty
[bar]	[ms]	[min]	[g]	[g]	[g]	[mg/s]	[%]
3	30	2	40.48	52.31	11.82	98.53	12
3	30	2	40.85	52.57	11.72	97.69	12
3	30	2	52.57	64.39	11.82	98.53	12
3	15	3	40.78	49.59	8.81	48.92	6
3	15	3	40.93	49.77	8.84	49.09	6
3	45	2	41.04	58.78	17.73	147.78	18
3	45	2	40.91	58.64	17.73	147.76	18
3	60	1.5	40.90	58.60	17.70	196.67	24
3	60	1.5	40.93	58.81	17.88	198.66	24
5	1	3	40.88	41.52	0.64	3.56	0.4
5	1	3	40.86	41.52	0.66	3.65	0.4
5	5	2	40.91	43.40	2.49	20.71	2
5	5	2	40.78	43.26	2.48	20.70	2
5	15	2	40.80	48.38	7.58	63.16	6
5	15	2	40.73	48.30	7.57	63.11	6
5	30	2	40.77	55.93	15.17	126.38	12
5	30	2	40.67	55.93	15.25	127.12	12
5	45	1.5	40.81	57.92	17.10	190.04	18
5	45	1.5	40.77	57.94	17.17	190.78	18
5	60	1	40.79	56.12	15.33	255.49	24
5	60	1	40.74	56.07	15.34	255.60	24
4	30	2	40.76	54.39	13.63	113.62	12
4	30	2	40.78	54.40	13.62	113.52	12
4	60	1.5	40.67	61.21	20.54	228.22	24
4	60	1.5	40.69	61.18	20.49	227.71	24

The tests were performed for up to 5 minutes, depending on the expected flow rate. For the experiments using only water, a few points were also repeated to check for consistency in urea dosing. The result showed good repeatability between points, and that the duty cycle was the key factor for the average. Measured duty and flow for a set of tests are given in Table 7 and illustrated in Figure 20.

Table 7: Urea/water injector settings and calculated flow rates for a urea/water solution.

Measured Values						Calculated Values		
Pressure	Pulse	Frequency	Time	Weight before	Weight after	Δ Weight	Flowrate	Duty
[bar]	[ms]	[Hz]	[min]	[g]	[g]	[g]	[mg/s]	[%]
5	1	4	3	40.96	41.77	0.81	4.49	0.4
5	1	4	3	41.77	42.49	0.72	4.01	0.4
5	1	8	3	40.84	42.26	1.42	7.87	0.8
5	1	16	3	40.95	43.84	2.89	16.05	1.6
5	5	4	2	40.94	43.60	2.66	22.16	2
5	5	8	2	40.97	46.29	5.32	44.33	4
5	5	16	2	41.08	51.56	10.48	87.37	8
5	20	4	2	41.11	51.78	10.67	88.91	8
5	60	4	1	41.20	57.12	15.92	265.36	24
5	30	8	1	41.26	57.17	15.92	265.26	24
5	15	16	1	41.18	57.01	15.84	263.94	24
5	5	48	1	41.13	56.57	15.44	257.37	24
5	125	5	0.5	40.96	61.73	20.77	692.43	62.5
	15.62							31.2
5	5	20	0.5	41.18	51.62	10.44	348.04	5
5	1000	1	0.33	41.13	63.69	22.56	1128.15	100
5	1000	1	0.33	41.18	63.29	22.12	1105.81	100

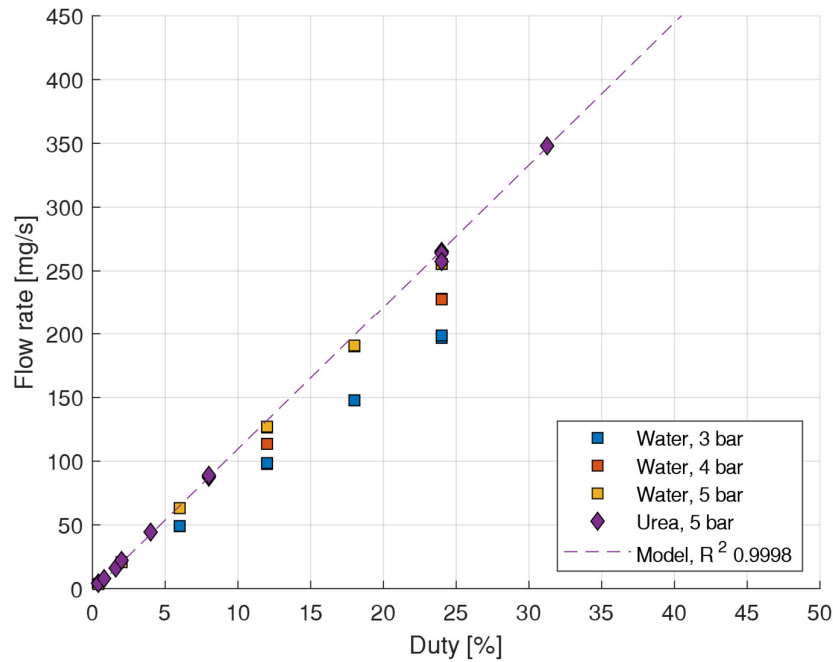


Figure 20: Urea/water flow rate as function of injector duty signal

Appendix 2: SCR Measured Data

Table 8: SCR measurement data upstream/downstream for the last respective measurement points of the day.

SCR Run		1 Low	1 High	2 Low	2 High	3 Low	3 High
GHSV	[h ⁻¹]	9,86E+04	9,86E+04	8,02E+04	8,02E+04	8,00E+04	7,95E+04
H ₂ O upstream	[%]	16,50	16,83	20,46	20,44	17,04	16,84
H ₂ O downstream	[%]	16,66	16,47	20,64	20,71	17,06	16,98
H ₂ O injected	[%]	0,04	0,05	0,19	0,26	0,04	0,07
NH ₃ injected	[ppm]	140,5	230,2	730,1	1091,1	152,9	246,0
NH ₃ downstream	[ppm]	0,2	12,5	0,3	36,6	0,0	4,0
NO _x upstream	[ppm]	149,1	199,2	1006,9	967,1	230,8	198,7
NO _x downstream	[ppm]	69,1	16,1	467,6	212,3	120,1	49,7
NO upstream	[ppm]	41,6	57,5	419,9	393,7	66,1	61,0
NO downstream	[ppm]	7,0	0,2	168,7	84,0	21,0	5,7
NO ₂ upstream	[ppm]	107,4	141,4	519,2	519,4	162,8	137,4
NO ₂ downstream	[ppm]	62,1	15,9	293,6	126,1	99,0	44,0
N ₂ O upstream	[ppm]	0,53	0,56	0,47	0,55	0,52	0,50
N ₂ O downstream	[ppm]	1,18	4,88	2,33	18,37	1,13	4,48
ANR	[-]	0,94	1,16	0,73	1,13	0,66	1,24
Temp. upstream	[°C]	283	279	294	264	247	247
Temp. downstream	[°C]	282	279	295	266	246	247
Fuel Flow	[kg h ⁻¹]	1,14	1,15	1,15	1,14	0,95	0,94
CO ₂ upstream	[ppm]	282,3	297,3	399,5	449,2	339,8	321,0
CO ₂ downstream	[ppm]	335,2	361,5	606,1	748,9	366,6	405,3
CO ₂ injected	[ppm]	61,5	76,7	273,8	380,1	56,6	95,6
CO upstream	[ppm]	0,09	0,15	0,17	0,04	0,05	-0,06
CO downstream	[ppm]	0,66	0,51	0,85	0,57	0,24	0,08
ΔNO _x	[ppm]	-79,9	-183,1	-539,3	-754,8	-110,8	-149,0
ΔNO	[ppm]	-34,6	-57,4	-251,2	-309,7	-45,1	-55,3
ΔNO ₂	[ppm]	-45,3	-125,5	-225,6	-393,3	-63,7	-93,4
ΔN ₂ O	[ppm]	0,65	4,31	1,86	17,82	0,62	3,98
ΔNH ₃	[ppm]	-140,3	-217,6	-729,9	-1054,5	-153,0	-241,9
NO ₂ /NO _x upstream	[-]	0,72	0,71	0,52	0,54	0,71	0,69
NO ₂ /NO _x downstream	[-]	0,90	0,99	0,63	0,59	0,82	0,89
NO _x Conv.	[%]	53,6	91,9	53,6	78,1	48,0	75,0
NO Conv.	[%]	83,2	99,7	59,8	78,7	68,2	90,7
NO ₂ Conv.	[%]	42,1	88,7	43,5	75,7	39,2	68,0

Appendix 3: Additional SCR plots

SCR Point 1

During the SCR runs, the FTIR was allowed to measure continuously, while measurements from the AMA i60/PUMA/Dewesoft systems was taken as frequently as possible. The sampling point of the FTIR was switched between the downstream positions (SP2), where data concerning conversion efficiency etc could be collected, and the upstream position (SP1), which was used periodically to check the total NO_x level going into the catalyst as well as the NO_2/NO_x ratio. Figure 21 shows the results from the first case for a low ANR target at 0.8. The top graph shows nitrogen oxide species measured by the FTIR and AMA i60. The middle graph shows the ammonia slip and N_2O generation, while the bottom graph indicates the sampling point of the FTIR system and the calculated ANR based on the engine out NO_x levels measured by the AMA i60 CLD.

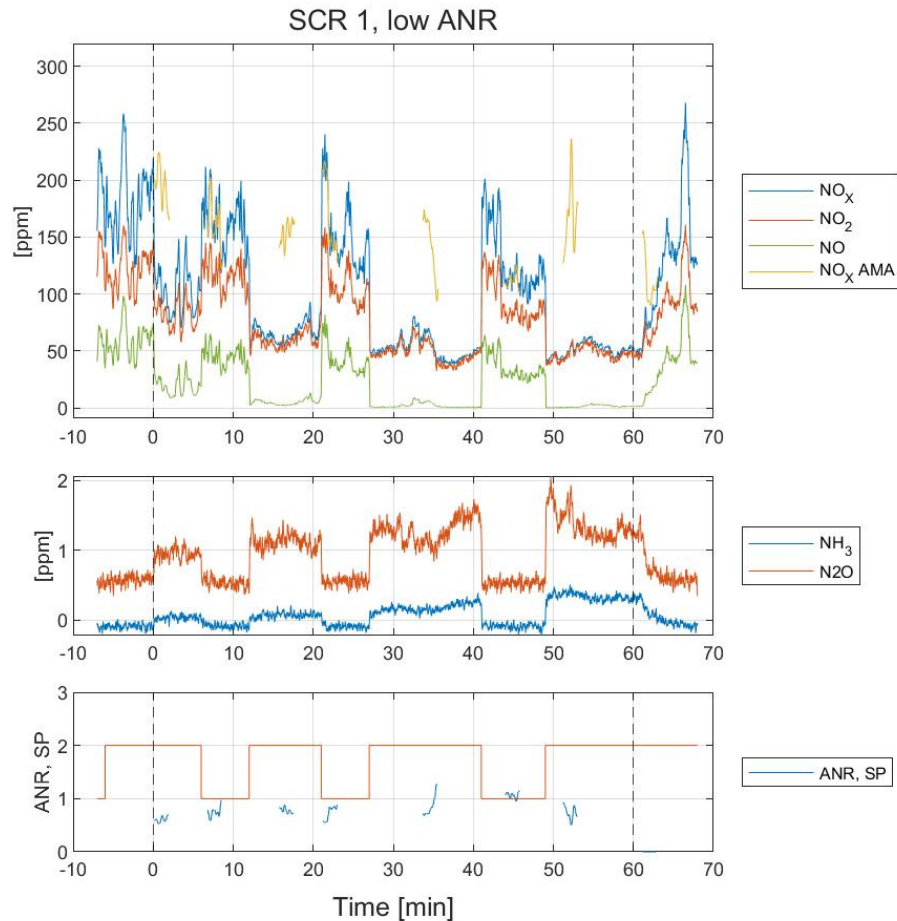


Figure 21: Detailed results from the first SCR case, with low ANR target of 0.8.

The results highlight a difficulty in reaching the target ANR, as the engine out NO_x levels are not stable over time. As such, the ANR varies with time. The levels just before the start of urea injection, which was the time the duty of the injection system was calculated, showed higher NO_x than later in the measurement, and led to an

overestimation of the NH_3 required. Calculating the correct urea amount, given fuel flow and air flow through the engine and the engine out NO_x and adjusting the duty on the PWM generator is too time consuming to do in response to changing NO_x levels. As a result, the ANR level was above 1 for periods of time, between approximately 15:50 and 16:20. This means that the average numbers reported Appendix 2 may be slightly skewed, as the points with lower ANR will have a lower NO_x conversion, while the periods with ANR over one may have a higher conversion. Overall, the SCR system showed a strong reduction in NO , while reduction of NO_2 proved more difficult. The incoming NO_2/NO_x ratio was also higher than what is generally accepted as optimal for a conventional SCR system and excluded complete use of the fast NO_x reduction pathway.

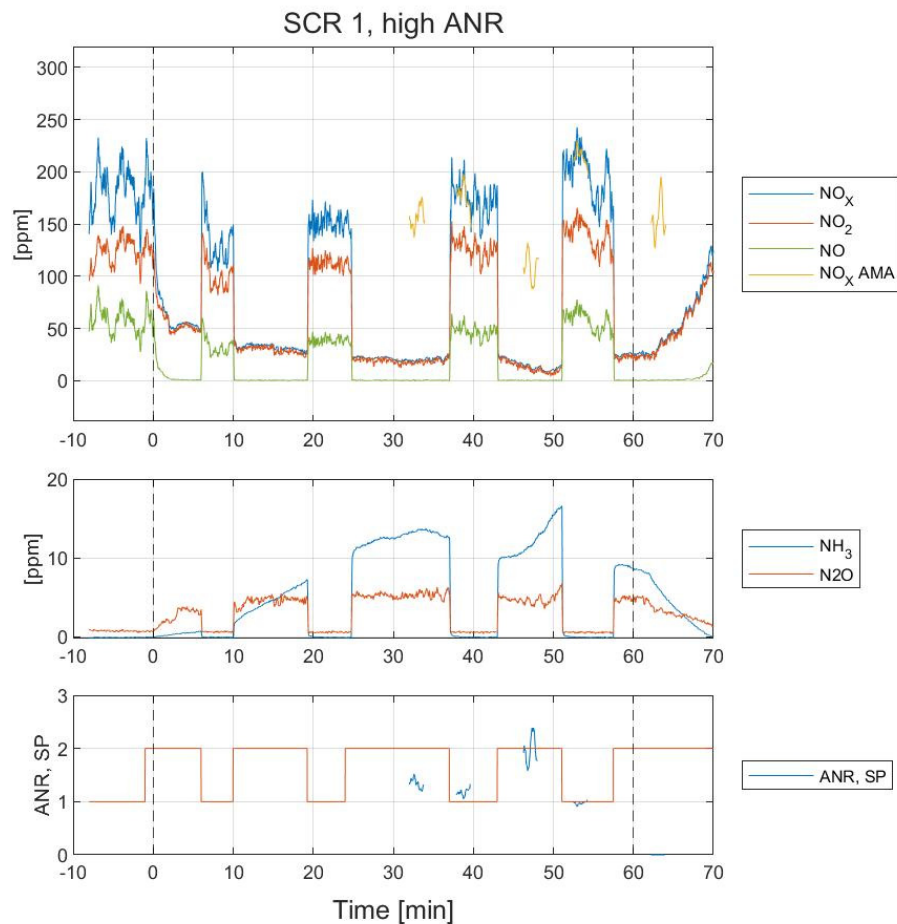


Figure 22: Detailed results for the first SCR case, with high a target ANR of 1.2.

For the high ANR run for case 1, shown in Figure 22, a higher conversion of nitrogen oxides was noticed. The NO_x levels, just like in the low ANR case, was unstable and caused a slight overestimation of the NH_3 injected, compared to the target ANR of 1.2. The actual ANR was found to be between 1 and 1.5. The actual goal of having an excessive ANR was however reached, and an expected slip of ammonia could be observed. The ammonia slip increased slightly over time, most likely as the catalyst slowly saturated with ammonia. Storing of ammonia in the SCR catalyst is confirmed by

the slow release of ammonia after the injection is stopped. As storage of NH_3 occurred, a continued reduction of NO_x emissions can be seen for up to approximately 15 minutes after the injection is stopped. This effect was not pronounced in the case of the lower ANR.

SCR Point 2

For case 2, which is the low intake pressure, high speed case, a significantly higher engine out NO_x level is observed. The levels did however appear to more stable than in cases 1 and 3, which made reaching and maintaining the target ANR more successful. The ANR was however slightly lower than intended. The measured emissions as well as the injected urea, ANR and sampling points show in Figure 23.

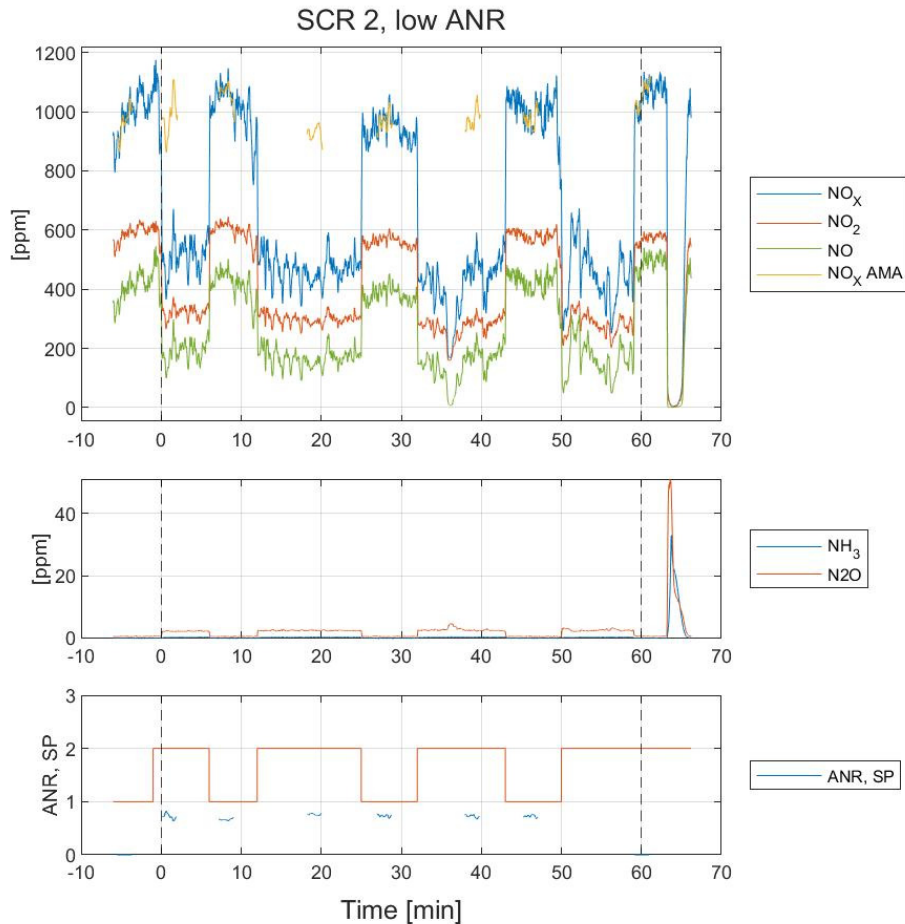


Figure 23: Detailed results from SCR case 2, ANR target at 0.8.

At the higher NO_x levels and water content, one of the main differences in composition is the NO_2/NO_x ratio, which is closer to the ideal. The reason for this is the lower relative oxidation of NO into NO_2 at the DOC in this case. One of the main effects this has on the downstream emissions is that there is more NO present, shown in the light blue line in Figure 23.

Another difference compared to cases with lower NO_x going into the catalyst, is that the time response of the catalyst seems faster. When compared to case 1 with low ANR (Figure 21) the NO_x shows a faster response to urea injection at the start of the period, and a faster return to pre-SCR levels as the urea injection is stopped. The effect must be due to the high concentration of NO_x and NH_3 , and not space velocity, as the GHSV is around 20% lower.

SCR Point 3

Case 3, which should produce similar exhaust gas compositions to case 1, showed lower NO_x conversion. Lower emissions of nitrous oxides in the period before sampling led to a slight underestimation of the needed duty of the urea injection system, and the ANR was lower than for the corresponding target ANR in case 1, which may make comparison of the total conversion efficiency between the cases difficult. The incoming NO_2/NO_x ratio is also slightly lower, which may be caused by the lower oxidation in the DOC. This in turn is most likely due to the lower temperature in the exhaust at lower space velocity. The corresponding increase in residence time in the exhaust may give more time for heat losses to the environment, and correspondingly lower exhaust temperatures going into the catalysts.

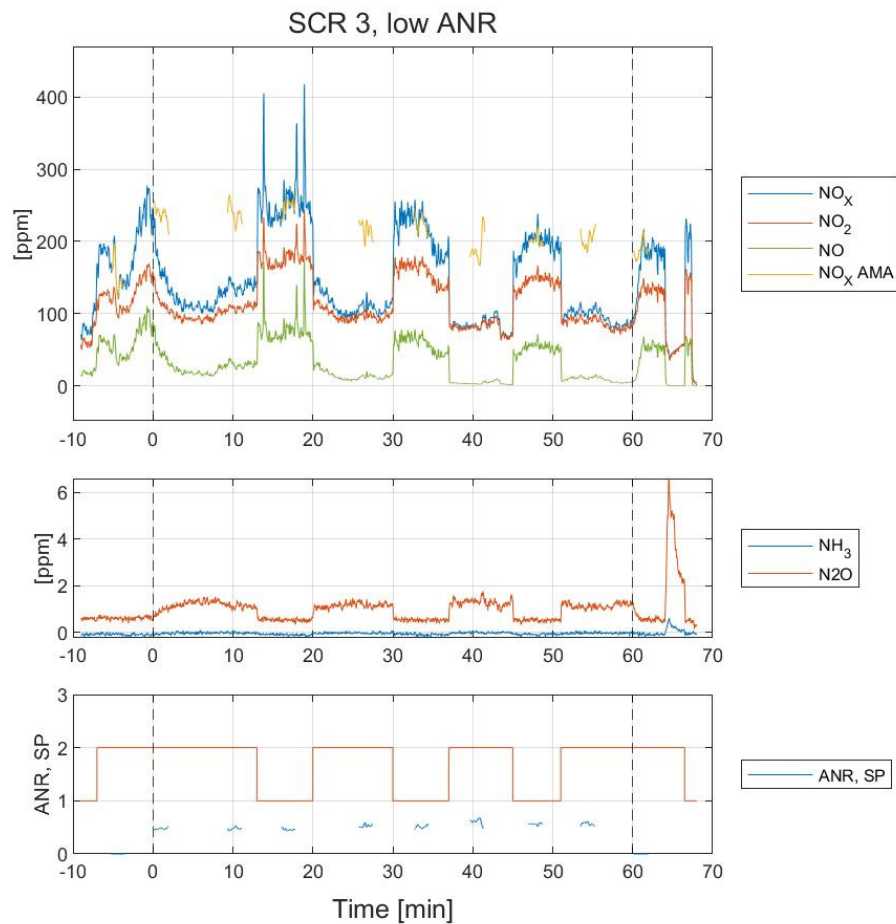


Figure 24: Detailed results from SCR case 3, low ANR target of 0.8.

Figure 24 shows the emissions from the low ANR run for case 3. While the gas composition downstream of the DOC did not change noticeably compared to case one, the downstream shows lower reduction of total NO_x. The biggest discrepancy with the results from the previous cases is that there is a lower reduction of NO compared to case 1 with low ANR. While the lower total reduction can in part be caused by the lower ANR, the reduction in NO₂ is closer to the level observed in case 1 than the reduction in NO. Thus, the biggest difference in the NO_x reduction performance is in the capability to reduce NO, which for the other cases seems to have been the easiest component to process in the EATS.

For the high ANR run in case 3, the NO_x reduction was lower than in case 1 with high ANR. Again, the NO₂/ NO_x ratio is lower, meaning that the performance when it comes to reducing NO is relatively weaker than the performance in reducing NO₂, given that the upstream ratios are similar in case 1 and case 3. The results are shown in Figure 25.

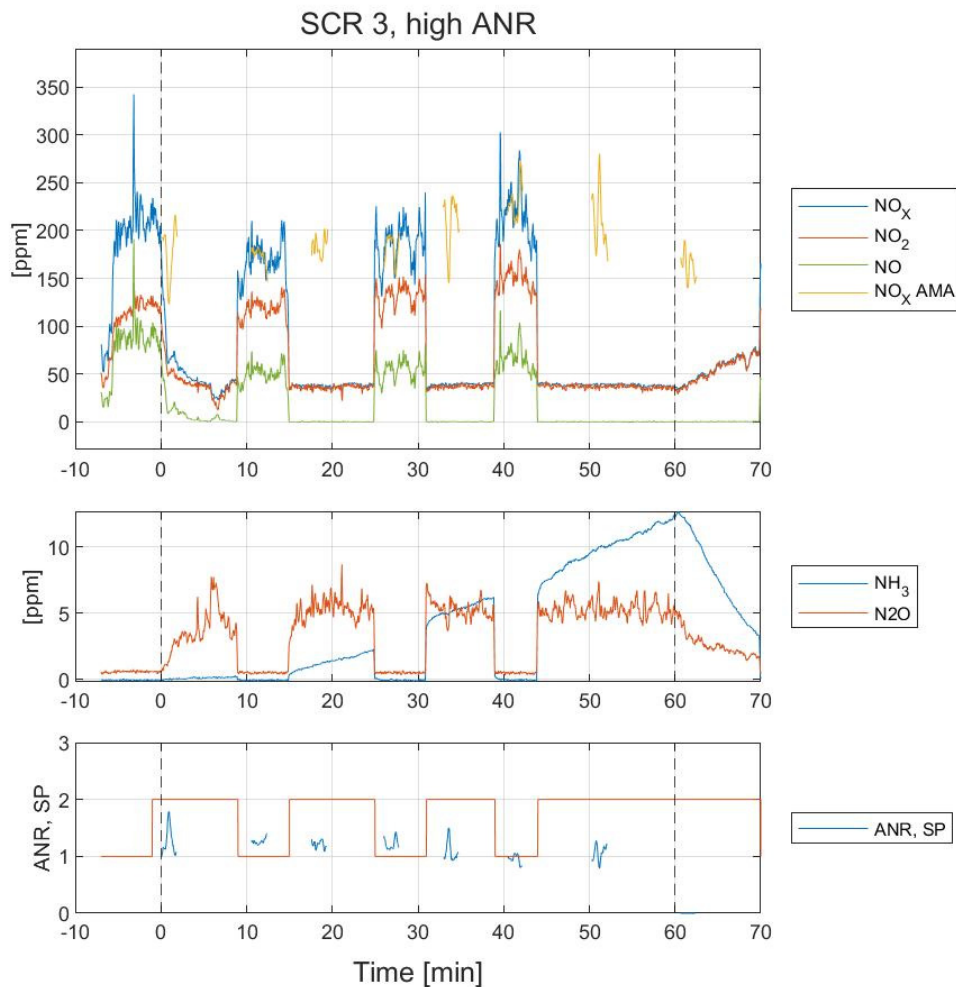


Figure 25: Detailed results from SCR case 3, high ANR target of 1.2.

Appendix 4: Model Data for Catalyst

The models used to fit the data in the paper and to predict the NO₂ to NO_x ratio downstream of the oxidising catalyst when the FTIR was measuring downstream of the SCR catalyst are given in the tables below. In general, the model for NO₂ to NO_x ratio show good R2 values, while the NO and NO₂ conversion efficiency models show a worse fit to data, possibly caused by the additional error source of the modelled NO₂/NO_x ratio used in them.

Table 9: Model details for the NO₂ to NO_x ratio downstream of oxidising catalyst

NO ₂ /NO _x after oxy-cat	Coeff. SC	Std. Err.	P	Conf. int(±)
Constant	0.6156	0.0133	4.93E-35	0.0269
T OC	0.0020	0.0096	0.838374	0.0194
NO _x engine out	-0.2018	0.0277	1.02E-08	0.0561
H ₂ O	0.0145	0.0187	0.444102	0.0378
TOC ²	-0.0160	0.0038	0.000144	0.0077
(NO _x) ²	0.0470	0.0115	0.000227	0.0233
N = 44	Q2 =	0.8820	Cond. no. =	21.1300
DF = 38	R2 =	0.9610	RSD =	0.0325
Comp. = 5	R2 adj. =	0.9560	Confidence =	0.9500

Table 10: Model details for the NO conversion efficiency in SCR catalyst

NO conv. efficiency	Coeff. SC	Std. Err.	P	Conf. int(±)
Constant	100.11	8.63	6.88E-09	18.40
T SCR	0.93	4.35	0.834276	9.27
ANR	15.90	2.87	5.63E-05	6.11
NO ₂ /NO _x	2.15	6.39	0.741147	13.62
T SCR ²	-18.58	4.18	0.000469	8.90
ANR ²	-6.46	1.97	0.004969	4.19
(NO ₂ /NO _x) ²	1.82	9.25	0.846841	19.72
N = 22	Q2 =	0.60	Cond. no. =	13.49
DF = 15	R2 =	0.84	RSD =	10.47
Comp. = 3	R2 adj. =	0.77	Confidence =	0.95

Table 11: Model details for the NO₂ conversion efficiency in SCR catalyst

NO ₂ conv. efficiency	Coeff. SC	Std. Err.	P	Conf. int(±)
Constant	76.30	5.95	0.00	12.68
T SCR	-2.68	3.00	0.39	6.39
ANR	21.67	1.98	0.00	4.21
NO ₂ /NO _x	-3.94	4.41	0.39	9.39
T SCR ²	-11.89	2.88	0.00	6.13
ANR ²	-4.63	1.35	0.00	2.89
(NO ₂ /NO _x) ²	-2.53	6.38	0.70	13.59
N = 22	Q2 =	0.75	Cond. no. =	13.49
DF = 15	R2 =	0.92	RSD =	7.21
Comp. = 3	R2 adj. =	0.88	Confidence =	0.95

Table 12: Model details for the NO_x conversion efficiency in SCR catalyst

NO _x conv. efficiency	Coeff. SC	Std. Err.	P	Conf. int(±)
Constant	81.26	2.45	1.91E-15	5.23
T SCR	-1.25	1.65	0.460621	3.53
NO _x upstream	5.32	1.81	0.010229	3.86
ANR	17.74	1.62	1.43E-08	3.44
T SCR ²	-13.12	1.96	7.26E-06	4.18
ANR ²	-4.52	1.04	0.000575	2.22
T SRC*NO _x	-3.11	1.42	0.044049	3.02
N = 22	Q2 =	0.86	Cond. no. =	5.55
DF = 15	R2 =	0.94	RSD =	5.64
Comp. = 3	R2 adj. =	0.91	Confidence =	0.95